![NR Norsk Regnesentral — Norwegian Computing Center]
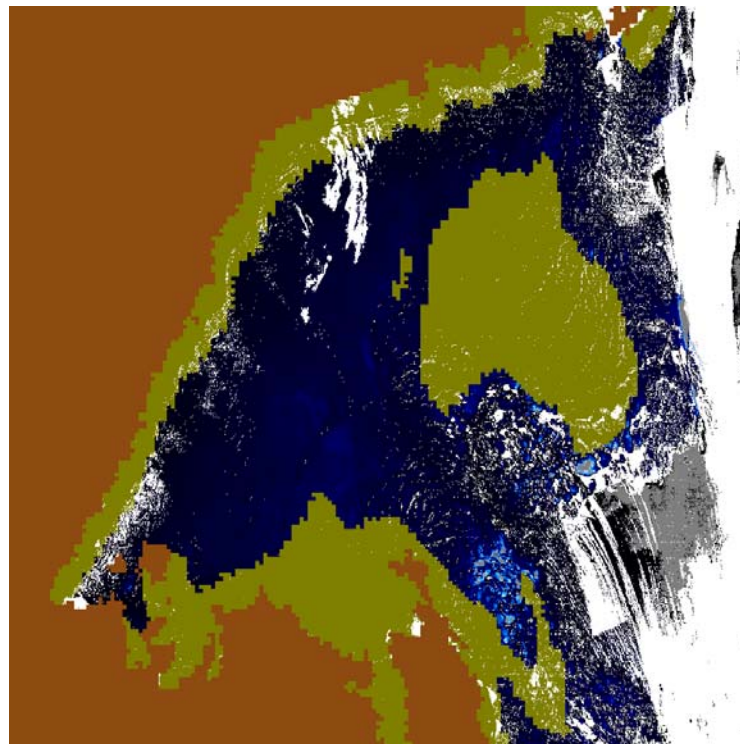
Note

Retrieval of thin sea ice thickness from thermal optical data

***Thinlce* project deliverables D1, D2 and D3**

Note no   **SAMBA/27/11**

Authors   **Øystein Rudjord, Øivind Due Trier and Rune Solberg**

Date   **8 August 2011**

Norsk Regnesentral

Norsk Regnesentral (Norwegian Computing Center, NR) is a private, independent, non-profit foundation established in 1952. NR carries out contract research and development projects in the areas of information and communication technology and applied statistical modelling. The clients are a broad range of industrial, commercial and public service organizations in the national as well as the international market. Our scientific and technical capabilities are further developed in co-operation with The Research Council of Norway and key customers. The results of our projects may take the form of reports, software, prototypes, and short courses. A proof of the confidence and appreciation our clients have for us is given by the fact that most of our new contracts are signed with previous customers.

Title	**Retrieval of thin sea ice thickness from thermal optical data**
Authors	**Øystein Rudjord, Øivind Due Trier and Rune Solberg**
Date	8 August
Year	2011
Publication number	SAMBA/27/11

Abstract

In the *ThinIce* project we explore the possibility of estimating the extent and thickness of thin sea ice by use of thermal optical data from the MODIS instrument on the Aqua satellite. In particular we investigate the feasibility of developing an operational algorithm for estimating the thickness of thin ice (TTI). We use a method based on modelling the heat balance on the sea ice surface. For night images we include models for the conductive heat flux and both the up-welling and down-welling long-wave heat flux, while the short-wave heat flux, latent heat flux and turbulent sensible heat flux are assumed to be negligible. For daytime images, short-wave heat flux is also modelled. Air temperature data is acquired from the ERA interim reanalysis dataset. We also implement an algorithm for masking out areas with thick ice, the thick ice mask (TIM). This algorithm uses microwave data from the AMSR-E instrument, also on the Aqua satellite.

The algorithms are tested on a time series of data from the Sea of Okhotsk, where TTI and TIM are evaluated and compared with each other and with sea ice concentration maps. A short test is also performed on the area around the Laptev Sea, where the estimates are compared with thin ice thickness estimates from SMOS. The algorithm is found to be promising, but several challenges are identified. In particular, we point out the unreliability of the cloud mask for the night images, and the errors introduced when modelling short-wave heat flux for daytime images. The accuracy is also found to be somewhat low, but with a significant potential for improvement.

Contents

1 Introduction

1.1 Background

Sea ice plays an important role in the climatic system, being a factor affecting the global energy budget as well as the oceanic circulation (Oliver 2005). It is also an indicator variable of climate change (ACIA 2005). Considering various types of sea ice, thin ice is of particular interest as it is most vulnerable to summer sea ice melt, and it allows for more heat transfer. The current trend in the Arctic towards more first-year ice and less multi-year ice implies a development towards a situation where thin ice will occur more frequently (Tucker et al. 2001; Comiso 2002). The quantification and monitoring of this ice type is therefore expected to become more important in the future.

Earth observation methods for the retrieval of sea ice concentration are accurate and well validated for multi-year ice and established first-year ice, but are less reliable and accurate for the younger stages of sea ice development (Comiso et al. 1997). Standard passive microwave algorithms for sea ice concentration, for instance, tend to confuse thin ice with a mixture of thick ice and open water, and are thus biased towards underestimation of the ice concentration.

Yu and Rothrock (1996) describe a promising method for the thickness retrieval for thin sea ice based on optical thermal data. The main idea is that the sea ice thickness is inversely proportional to the vertical temperature gradient through the ice, up to a thickness of about 0.5 m. The ice surface temperature is retrieved from thermal satellite data and is combined with meteorological data (air temperature and wind) in order to estimate the vertical temperature gradient, and thus the ice thickness.

1.2 Objectives

Within this project, *ThinIce*, we will examine whether this approach is a useful way towards an operational algorithm for monitoring and quantifying thin sea ice. Both the identification of the sea ice extent as well as the retrieval of its thickness are important variables that will be addressed.

The overall objective of the project is to develop a pre-operational multi-sensor algorithm for retrieval of the thickness of first-year sea ice from satellite data. The sub-objectives of the project are:

1. To determine whether first-year sea ice thickness can be retrieved from satellite data

2. If sea-ice thickness can be retrieved, then to develop an operational retrieval algorithm

If thin sea ice thickness retrieval from satellite data is successful, it will make global monitoring of this variable possible. This means that thickness and variability of the thickness over time for the first time could be observed operationally. Operational thin sea ice thickness monitoring will make improved energy balance modelling possible, which is in particular important for modelling the processes in the Arctic and Antarctica. In most climate models, energy balance processes in these areas are very much simplified. Improved climate modelling in polar areas could potentially have a significant impact on long-term climate change projections on the global scale. Furthermore, the area extent of thin sea ice is an important indicator of climate

change when measured systematically over time. Sea ice trend analysis could be significantly improved by operational use of the algorithm, providing significantly more accurate trend information on the global, regional and local scale.

For operational implementation, the algorithm could be adapted and implemented for the Sentinel-3 mission's SLSTR temperature radiometer. A multi-sensor approach combining optical and microwave data might have the largest potential, which may be considered later.

Norway is in an excellent position for exploitation of an operational algorithm for thin sea ice. The Norwegian Meteorological Institute is currently providing daily hemispherical sea ice concentration products based on the EUMETSAT SAF collaboration. A climate product service is currently under development in the PRODEX CryoClim project where the Ocean Sea Ice SAF daily products are utilised. Operational provision of thin sea ice products could very well be implemented within the framework of the CryoClim service.

1.3 Aim of this report

This document reports on the results from ThinIce work package 2, 3 and 4, deliverables D1, D2 and D3, respectively. A first version of a prototype algorithm has been implemented, to some degree building on NR's snow surface temperature experience using MODIS (Amlien and Solberg 2003). The algorithm uses MODIS data for thickness retrieval and cloud masking, and AMSR-E data for detection of areas suspected to represent thin ice. Valuable experience on sea ice retrieval has been shared with us by Georg Heygster, University of Bremen, and his research group. The work is also building on a non-funding collaborative research agreement (AO) with JAXA, the GCOM project "Retrieval of sea ice types and properties from AMSR2 and MODIS", which is, led by Georg Heygster (PI 106). In situ observations of ice thickness will hopefully be made available for the Sea of Okhotsk through this project.

2 Methodological approach

2.1 Thickness of thin ice (TTI)

The methodological approach for estimation of the ice thickness from optical thermal data combined with ancillary meteorological data is presented in the following. The ice thickness estimation approach follows Drucker et al. (2003) and Yu and Rothrock (1996) in that it is assumed that the ice is thin, the water temperature is at freezing level, and the temperature profile is linear within the ice. The heat flux through the ice is set equal to the atmospheric flux, which allows us to solve for what we call the thermal ice thickness h_T. According to Yu and Rothrock (1996), this linear approximation is valid for ice thicknesses less than about 0.5 m.

According to Yu and Rothrock 1996, the total heat flux on the top surface during the cold season can be decomposed into:

$$F_{total} = F_r - F_l^{up} + F_l^{dn} + F_s + F_e + F_c \tag{1}$$

Where F_r is the solar radiation flux, F_l^{up} is the upwelling long-wave flux (the blackbody radiation from the surface), F_l^{dn} is the downwelling longwave radiation (the blackbody radiation from the atmosphere on the surface), F_s is the turbulent sensitive heat flux, F_e is the latent heat flux and F_c is the conductive heat flux (the heat flux from the water to the surface). We will assume that the surface temperature can be considered constant, giving $F_{total} = 0$. Initially, we will only consider night scenes, where the solar radiation is vanishing, $F_r = 0$. As a first approximation we will also assume $F_s = F_e = 0$. According to Maykut (1978) these terms are significantly smaller than the incoming long-wave radiation.

The long-wave fluxes can be described by the Stefan-Boltzmann law for blackbody radiation, giving us $F_l^{up} = \varepsilon_i \sigma T_s^4$ and $F_l^{dn} = \varepsilon_a \sigma T_a^4$ where $\sigma = 5.6704 \cdot 10^{-8} \frac{\text{W}}{\text{m}^2 \text{K}^4}$ is the Stefan-Boltzmann constant, $\varepsilon_i = 0.97$ is the emissivity of ice, $\varepsilon_a = 0.7855$ is the effective emissivity of the atmosphere, and T_s and T_a are the temperatures of the ice surface and the atmosphere respectively. T_s can be estimated from the thermal bands of the MODIS images, and T_a is approximated to the air temperature at 2 meters. Re-analysis of air temperatures are provided by the European Centre for Medium-Range Weather Forecasts (ECMWF) through the ERA project (http://www.ecmwf.int/research/era).

We follow Yu and Rothrock in that we assume that the conductive heat flux, F_c, can be expressed as:

$$F_c = \frac{k_i k_s (T_f - T_s)}{k_s H + k_i h} \tag{2}$$

Here, k_i and k_s are the thermal conductivity of ice and snow, respectively, T_f is the freezing temperature of seawater, modelled as $T_f = -0.055 S_w$, where we have assumed the seawater

salinity to be $S_w = 31.0$ ppt. H is the thickness of the ice and h is the thickness of snow on top of it. The conductivity of snow was set to $k_s = 0.31$, and the conductivity of sea ice is assumed to be $k_i = k_0 + \beta S/(T_i - T_0)$. Here $k_0 = 2.034 \dfrac{\mathrm{W}}{\mathrm{mK}}$ is the conductivity of pure ice,

$\beta = 0.13 \dfrac{\mathrm{W}}{\mathrm{m^2 kg}}$, $T_0 = 273.15\mathrm{K}$ is the freezing point of pure water and T_i is the temperature within the ice. We assume this to be equal to the surface temperature $T_i = T_s$. S is the sea ice salinity, measured in parts per thousand (ppt.), and is modelled as

$$S = 14.24 + 19.39H \quad \text{for } H \le 0.4\,\mathrm{m} \tag{3}$$

$$S = 7.88 + 1.59H \qquad \text{for } H > 0.4\,\mathrm{m}$$

Also, we have assumed an empirical relationship between snow and ice thickness:

$$h = 0 \qquad\qquad \text{for} \qquad H \le 5\mathrm{cm}$$

$$h = 0.05H \qquad \text{for} \qquad 5\mathrm{cm} \le H < 20\mathrm{cm} \tag{4}$$

$$h = 0.1H \qquad\; \text{for} \qquad H \ge 20\mathrm{cm}$$

These assumptions are combined into (2) to describe the conductive heat flux, which is then inserted into (1) together with the upwelling and down-welling long-wave fluxes. For a given set of temperatures T_s and T_a this equation can be solved with respect to H.

T_s is found from thermal MODIS bands, using Key's algorithm for surface temperature (Key 1997). T_a is approximated for every MODIS pixel by using bilinear interpolation on the ERA temperature data (the ERA data has originally a resolution of only 1.5°, while the resolution of the MODIS images is 1 km). H is then estimated for each MODIS pixel for every regime in (3) and (4). The appropriate estimate for the sea ice thickness, H, is then selected based on the results.

Several masks are applied on the output. For masking out clouds the MODIS Cloud Mask product is used.

2.2   The solar radiation flux

The method may be extended to daytime images, by including a model describing the solar radiation heat flux F_r in eq. (1). As described in Yu & Rothrock (1996) we include two terms:

$$F_r = (1 - \alpha_S)F_{SW} - I_0 \tag{5}$$

Here F_{SW} is the incoming shortwave radiation, α_S is the surface albedo and I_0 is the radiation flux passing through the ice. The last term can be described as $I_0 = i_0(1 - \alpha_S)F_{SW}$ where the transmittance, i_0, is the fraction of the shortwave flux that passes through the ice. This leads to the solar radiation heat flux $F_r = (1 - \alpha_S)(1 - i_0)F_{SW}$.

For describing the shortwave heat flux, F_{SW}, we use a parameterisation by Zillman (1972), presented in Bisht et al. (2005), where $F_{SW} = S_0 \cos^2 \theta / d$, $S_0 = 1367 Wm^{-2}$ is the solar constant at the atmospheric top, θ is the solar zenith angle and $d = 1.085 \cos \theta + e_a (2.7 + \cos \theta) \times 10^{-3} + 0.1$. Here $e_a = f e_{sa}$ is the surface water vapour pressure, where e_{sa} is the saturation vapour pressure in hPa, and f is the relative humidity, assumed to be $f = 90\%$. The saturation vapour pressure is parameterised as a fourth order polynomial of the temperature as described in Maykut (1982):
$e_{sa} = aT^4 + bT^3 + cT^2 + dT + e'$. Here the coefficients are given as $a = 2.7798202 \times 10^{-6}$, $b = -2.6913393 \times 10^{-3}$, $c = 0.97920849$, $d = -158.63779$, $e' = 9653.1925$, and e_{sa} is in hPa.

Both the albedo, α_S, and the transmittance, i_0, of bare and snow covered ice can be parameterised as functions of ice or snow thickness, as described in Grenfell (1979), where they are found as $\alpha_S = 1 - A_1 \exp(-B_1 h) - C_1 \exp(-D_1 h)$ and
$i_0 = A_2 \exp(-B_2 h) - C_2 \exp(-D_2 h)$ where A_1, B_1, C_1, D_1, A_2, B_2, C_2, and D_2 are constants provided in Grenfell (1979) for bare and snow covered ice, and h is the snow or ice thickness. Unfortunately, inserting this exponential dependency of ice thickness into eq. (1) yields an equation of H which has no analytical solution. We therefore approximate them as constants within 4 intervals, corresponding to the regimes for salinity and snow thickness (see equations (3) and (4)). The constants are found as the mean values of the parameterised functions for α_S and i_0 on the relevant interval.

$\alpha_S = 0.0915710$ $i_0 = 0.641808$ for $H \leq 5\text{cm}$

$\alpha_S = 0.663315$ $i_0 = 0.604537$ for $5\text{cm} \leq H < 20\text{cm}$ (6)

$\alpha_S = 0.77793$ $i_0 = 0.254103$ for $20\text{cm} \leq H < 40\text{cm}$

$\alpha_S = 0.799825$ $i_0 = 0.0941154$ for $H \geq 0.4\,\text{m}$

Finally, the albedo, transmittance and shortwave heat flux is combined into eq. (5), which is then inserted into eq. (1), yielding a second order equation of H. The thin ice thickness can then be estimated using the procedure described above.

2.3 Thick ice mask (TIM)
Passive microwave data are used to narrow down areas of potential thin ice. New ice is distinguished from older (thick) ice by its spectral profile.
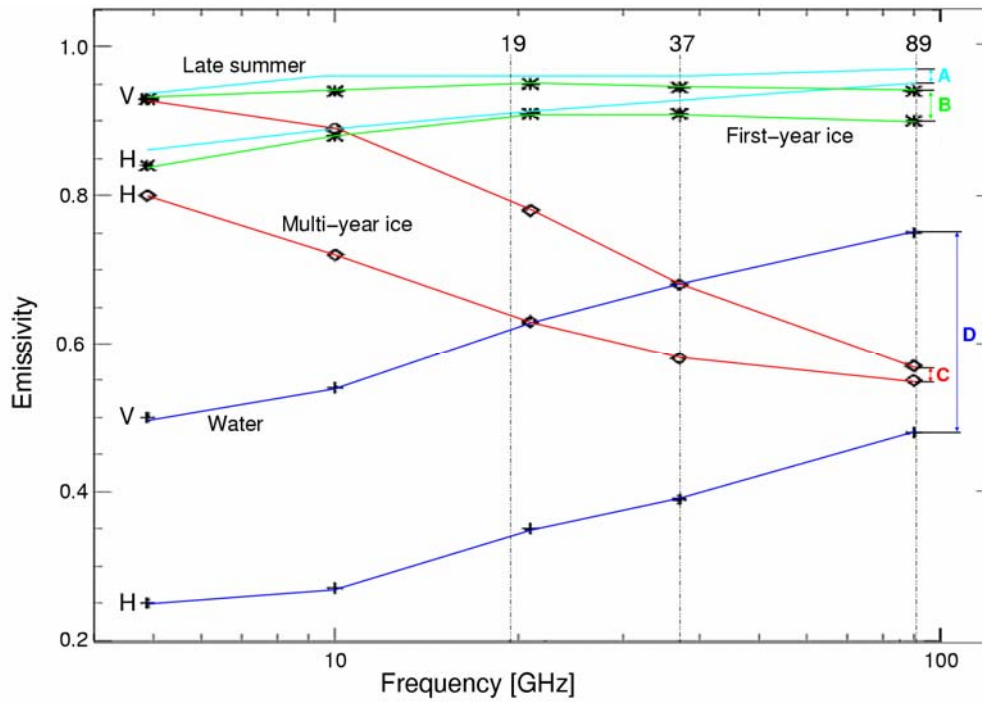
Figure 2.1: Spectral signature of water and sea ice.

Figure 2.1 shows the spectral profile of open water, first year ice and multi-year ice. We use a simple empirical relation to estimate potential thin ice. We use passive microwave data from two spectral points, 19 GHz and 89 GHz, both with vertical polarization. The ratio between the temperature brightness at these points indicates what we observe. $\frac{T_{89GHz}}{T_{19GHz}} > 1$ for open water, new ice, pancake ice and similar, while $\frac{T_{89GHz}}{T_{19GHz}} < 1$ for first year ice or multi-year ice (thick ice), where T_{89GHz} is vertically polarized passive microwave temperature brightness, at 89 GHz. Similarly, T_{19GHz} is vertically polarized temperature brightness at 19 GHz.

Therefore, a thick ice mask (TIM) is created, keeping only pixels where: $\frac{T_{89GHz}}{T_{19GHz}} > 1$. At this stage a land mask is also included, using the GSHHS shoreline data set (Wessel and Smith, 1996).

3 Processing chain

NR has developed a fully automated production chain, SnowLab, for Fractional Snow Cover products based on moderate resolution optical data. The system serves as a reference for the implementation of a fully operational high-performance operational system. The systems are coded in IDL using the ENVI environment.

Neither of the processing systems is intended for estimating ice thickness. However, much of the experience can be transferred to an ice thickness estimation system. A high-level conceptual diagram of the proposed Thickness of Thin Ice (TTI) processing chain is given in Figure 3.1.
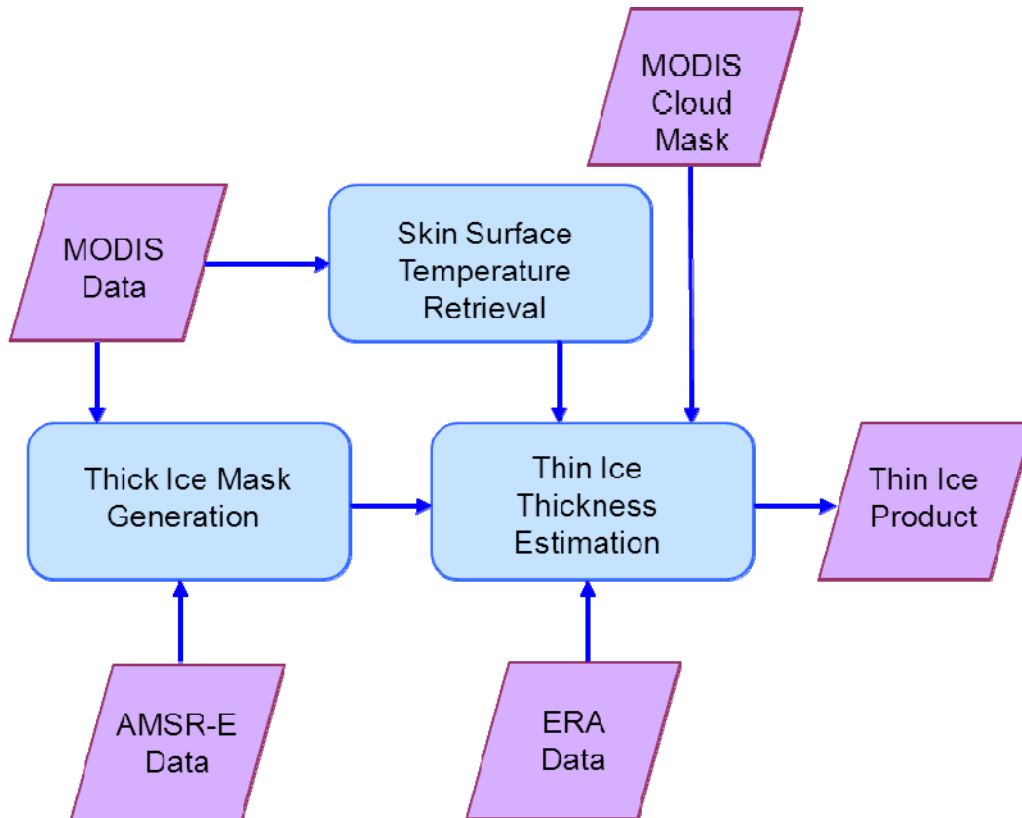
Figure 3.1: A diagram showing the processing chain.

The main data elements and modules of the processing chain are:

1. *MODIS data*: Aqua MODIS Level 1B data downloaded from NASA.
2. *AMSR-E data*: Aqua AMSR-E passive microwave brightness temperature data downloaded from NSIDC.
3. *Thick Ice Mask Generation*: Masking out land and old ice.
4. *Skin Surface Temperature Retrieval*: Estimating the surface temperature of snow and ice .
5. *MODIS Cloud Mask*: MODIS Cloud Mask product downloaded from NASA.
6. *ERA data*: Re-analyzed 2m air temperature data, downloaded from the ECMWF data server.
7. *Thin Ice Thickness Estimation*: Estimation of ice thickness based on surface and air temperatures. Applying masks.

8. *Thin Ice Product*: Map showing the extent and thickness of thin ice in ENVI format.

The Thick Ice Mask (TIM) is generated from the AMSR-E microwave data, using the vertically polarized 19 GHz and 89 GHz bands. During the same procedure land areas are also masked out. The resulting mask is resampled to the same geometry as the MODIS image. The MODIS latitude and longitude data are used as template.

Surface Temperature Snow (STS) is a module using the thermal MODIS bands to estimate the surface temperature of snow and ice in every pixel, using the algorithm developed by Key et al. (1997). The algorithm applies MODIS bands 31 (11μm) and 32 (12μm).

The *Thickness of Thin Ice (TTI)* is estimated using the algorithm described in chapter 2 of this document. The module reads an image of surface temperature data produced by STS and an ERA dataset containing 2 m air temperature. The air temperature is resampled to the same geometry as the STS image using bilinear interpolation. The mask produced by TIM is applied, as well as a MODIS cloud mask. The module produces a map showing the extent of thin ice, as well as its estimated thickness.

4 Experimental data set

The processing chain makes use of several data sets. First Aqua AMSR-E passive microwave data are used to narrow down our region of interest. We are using swath brightness temperature data (AE_L2A.2) of 38 km resolution. We use the vertically polarized 19 GHz and 89 GHz bands. These data can be downloaded from National Snow and Ice Data Center (NSIDC). The resulting mask is resampled to the same geometry as the MODIS data.

For re-analysed 2 m air temperature we have used the ECMWF ERA-Interim data. This has been obtained from the ECMWF data server (http://www.ecmwf.int/research/era). These data have only 1.5° resolution, which is very coarse, compared to the MODIS data (where we use 1 km resolution). The air temperature data are therefore resampled to the same resolution and geometry as the MODIS data, using bilinear interpolation.

The MODIS data are downloaded from NASA's LAADS Web (http://laadsweb.nascom.nasa.gov/data/search.html). We have used the level 1B calibrated radiances with a resolution of 1 km, and the level 2 cloud mask product. The latitude/longitude coordinates of the data are used as a geometric template for generating the thick ice mask. For estimating surface temperatures, the thermal bands are used. At the first test run we only make use of night images.

For testing of the algorithm we have analysed nightly images from the Russian coast by Sea of Okhotsk. We selected images bounded by 57° in north, 54° in south, 142° in west and 156° in east. In winter, the temperatures in this sea are low, with monthly average air temperatures in February between -7°C and 24°C depending on region. Because of this, the sea gradually fills with sea ice during the winter, starting in October and reaching it greatest extent in March. In summer the temperatures are warmer, with monthly average temperatures in August from 12°C to 18°C, leaving the sea ice free. This ensures that we do not have multi-year ice in our test data from this area. We have processed images from between December 15, 2008 and March 1, 2009.

We have also performed a test run on daytime images, after extending the algorithm to account for solar radiation flux as described in section 2.2. We used the same data types, geographical area and time frame as for the night time images, but in this case only used data acquired during day. However in this case we restricted the data set to a subset of the available images. We chose images where we expected less cloud coverage, and a certain amount of coastline based on the preview images on the MODIS webpage.

Figure 4.1: Test data are taken from Sea of Okhotsk (image from Google maps).

Finally a test has been performed in the Arctic in order to make a simple comparison with ice thickness results based on SMOS data. This is based on a released ice thickness estimate for October 13, 2010, provided by University of Bremen (Wang & Heygster, 2011). We chose to focus on an area by the northern coast of Russia, bound by 82° in north, 66° in south, 70° in west and 114° in east. We used images between October 11 and October 15, 2010. The algorithm was tested for both day and night images, on data which had some cloudless pixels.
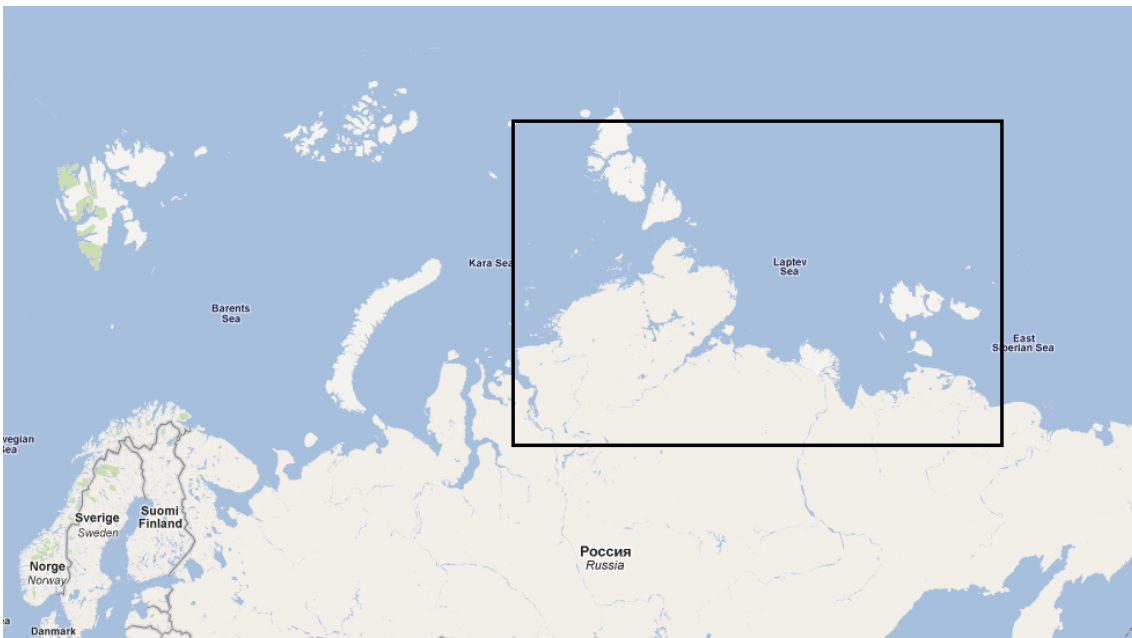
Figure 4.2: Arctic test data are taken from the area around the Laptev Sea (image from Google maps).

5 Experimental results

5.1 Night images

The algorithm produced a set of maps showing the estimated distribution and thickness of thin sea ice. Due to cloudy weather in the area, the amount of output is limited. Figures 5.1-5.9 show a selection of thin ice estimates from throughout the year. All show the Sea of Okhotsk, with exception of figure 5.8, which is centred on the Bering Sea.

5.1.1 First results

Figure 5.1 shows a typical result. The grey areas in the maps show where the thin ice model becomes invalid. This may happen when the condition of thermal equilibrium is not met, or when the estimated ice thickness is negative or greater than 2 m. In most cases, this means that the area contains open water. The ice extent is the combined blue (TTI) and green (TIM) area.
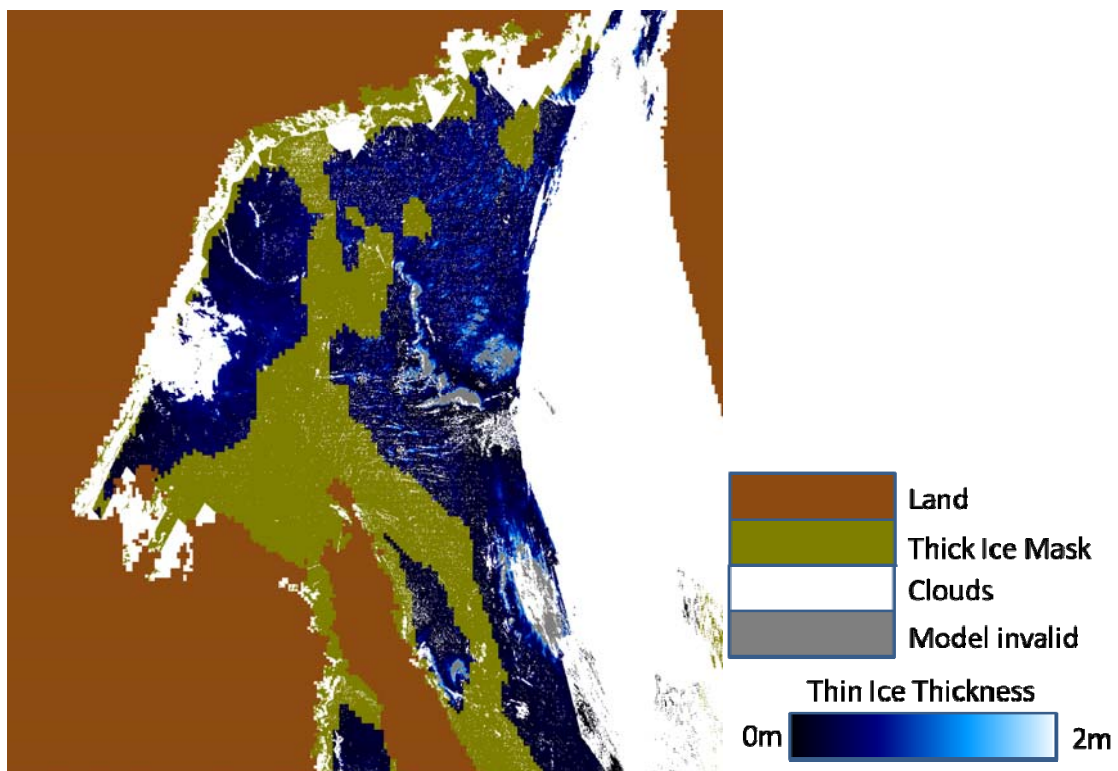
Figure 5.1: Sea of Okhotsk, February 25, 2009
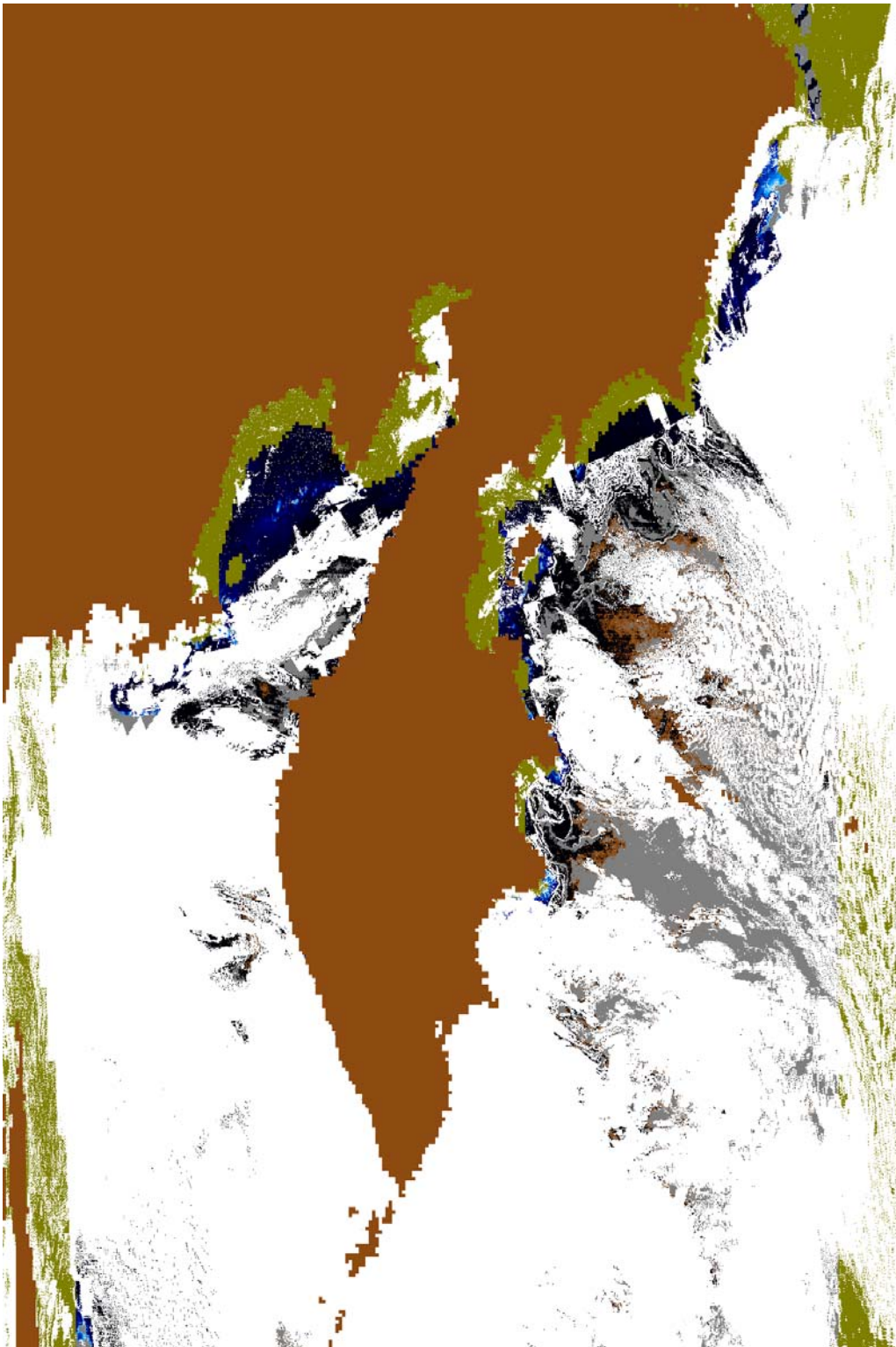
Figure 5.2: Kamchatka peninsula, January 27, 2009

Figure 5.2 demonstrates what happens when the model is at the border of validity. East of the Kamchatka peninsula there can be seen what appears to be some black and brown patterns in the water. The brown areas are not land in this case, but pixels where the algorithm failed to find a valid (real) solution. The areas appearing as black are actually very dark blue, representing extremely thin ice
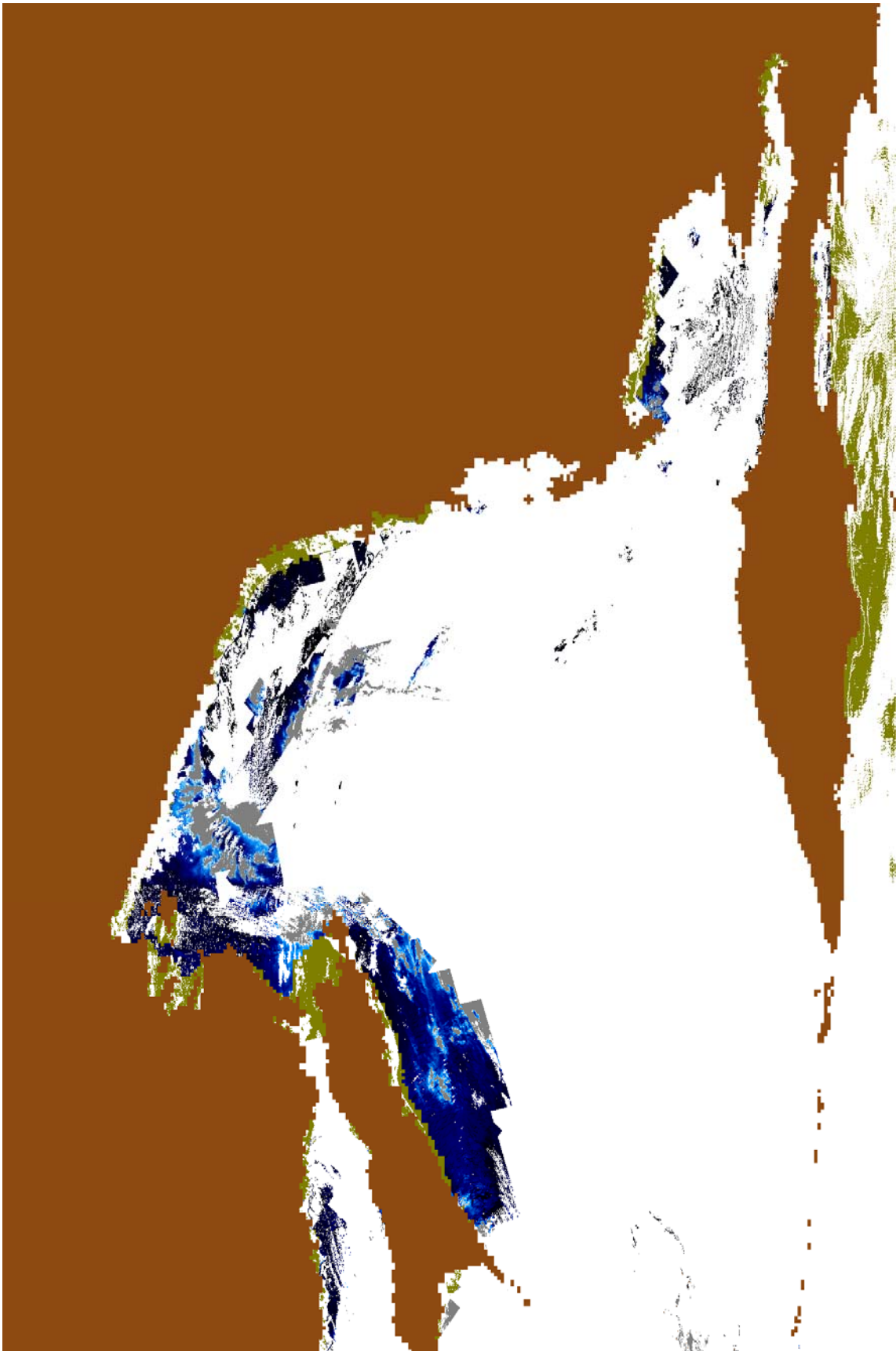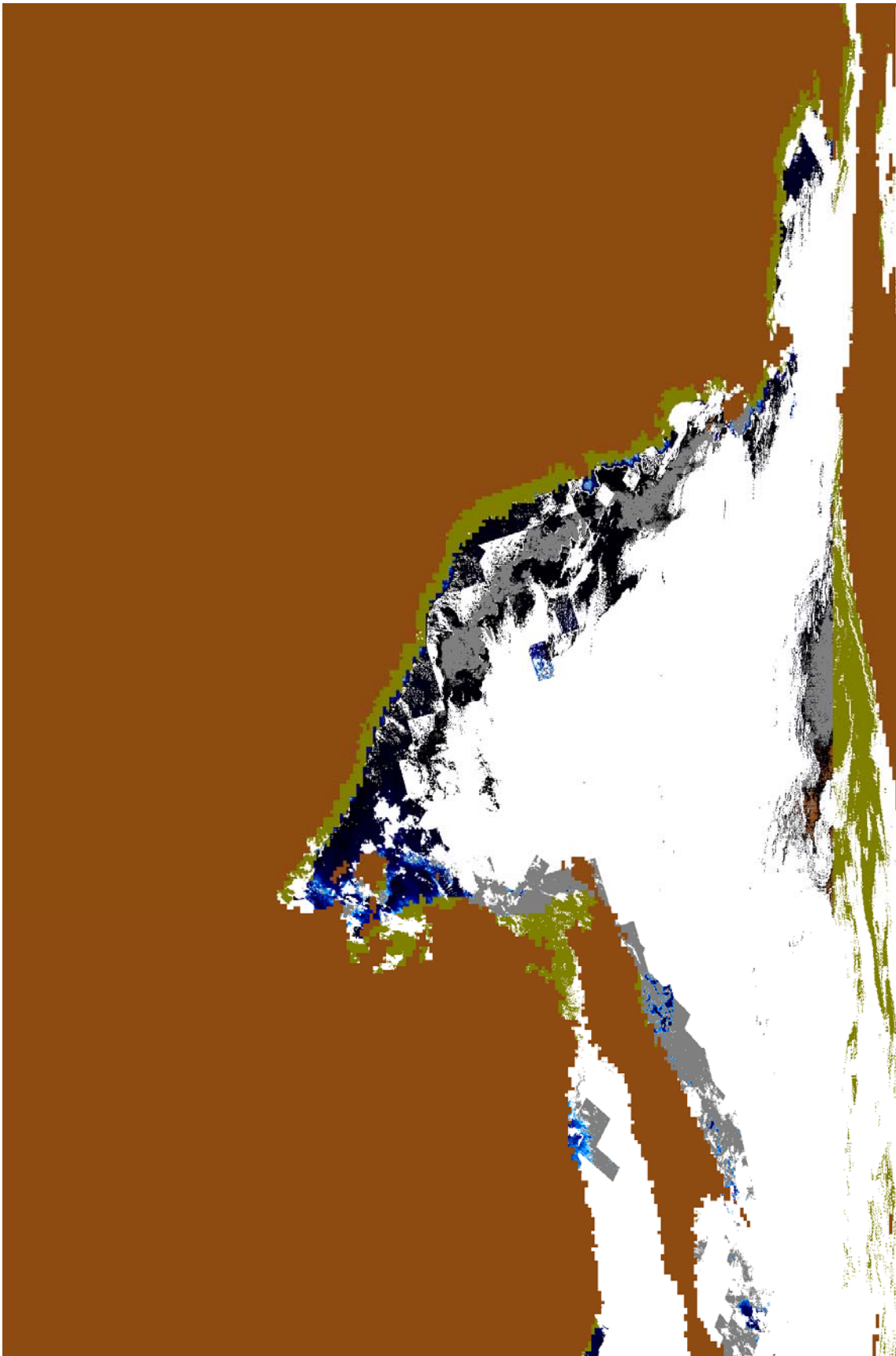
Figure 5.3: Sea of Okhotsk, December 25, 2008

Figure 5.4: Sea of Okhotsk, January 6, 2009

NR🌐 *ThinIce* **D1, D2, D3 - Retrieval of thin sea ice thickness from thermal optical data**
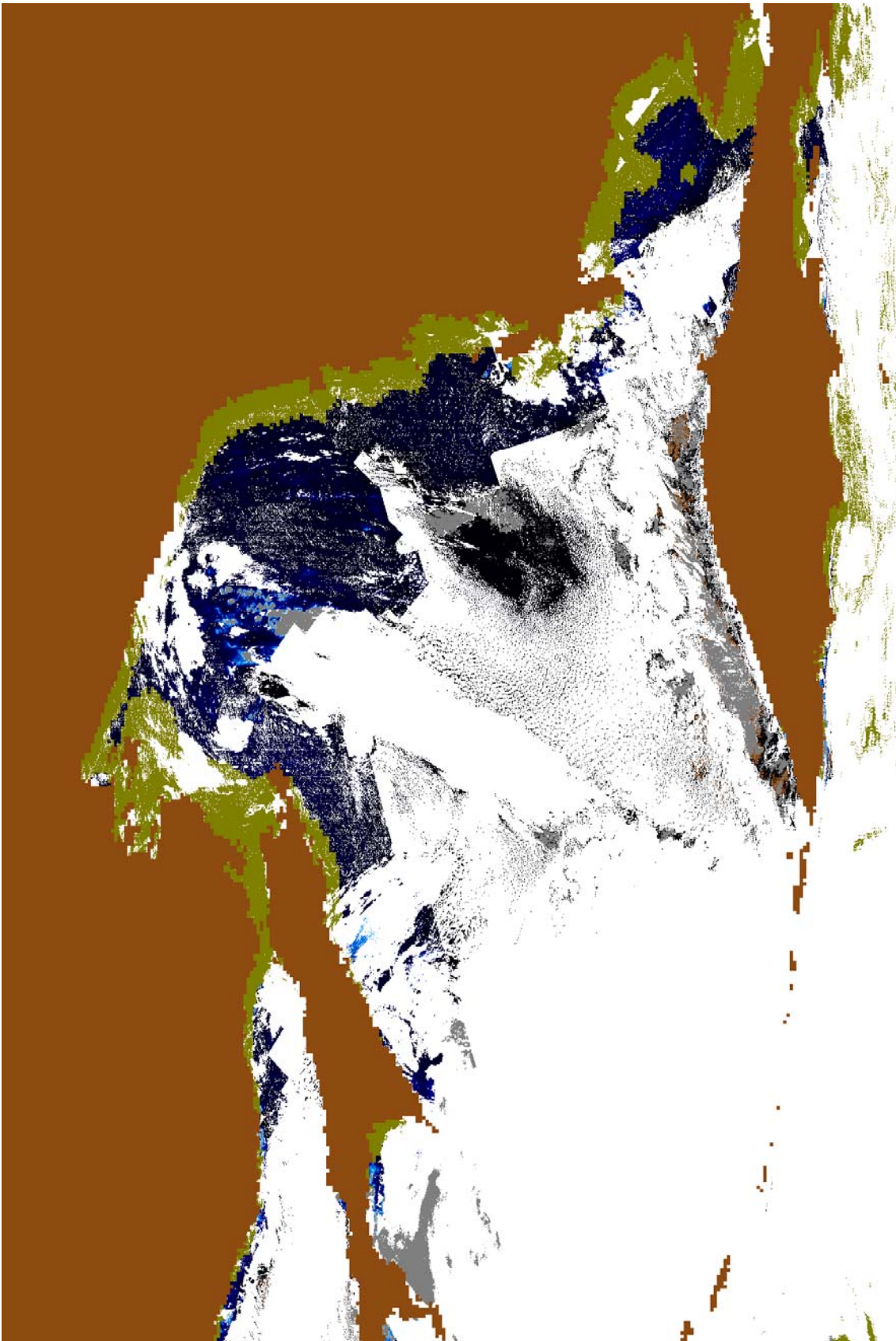
Figure 5.5: Sea of Okhotsk, January 19, 2009
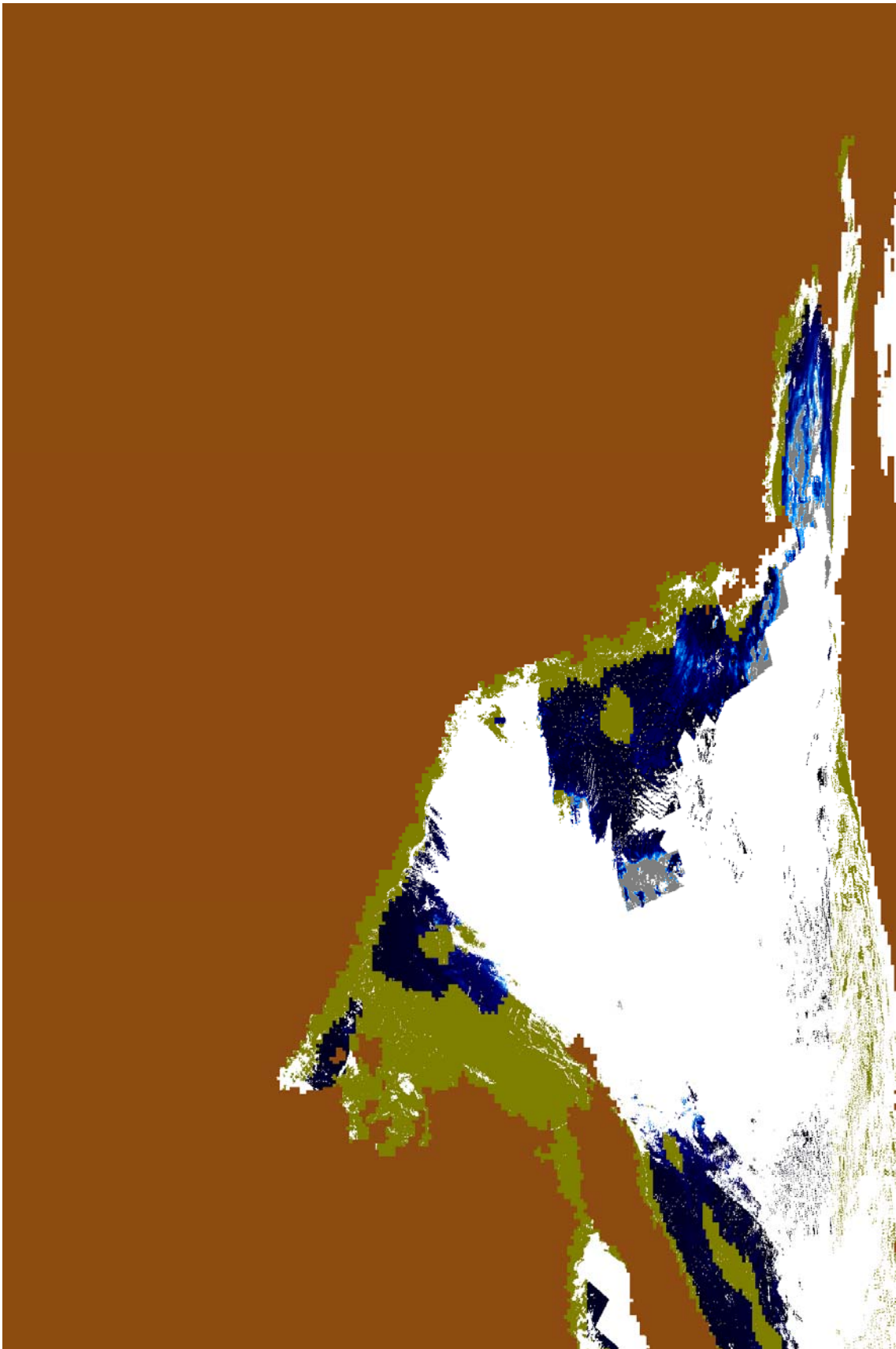
Figure 5.6: Sea of Okhotsk, February 7, 2009

NR🌐 *ThinIce* **D1, D2, D3 - Retrieval of thin sea ice thickness from thermal optical data**
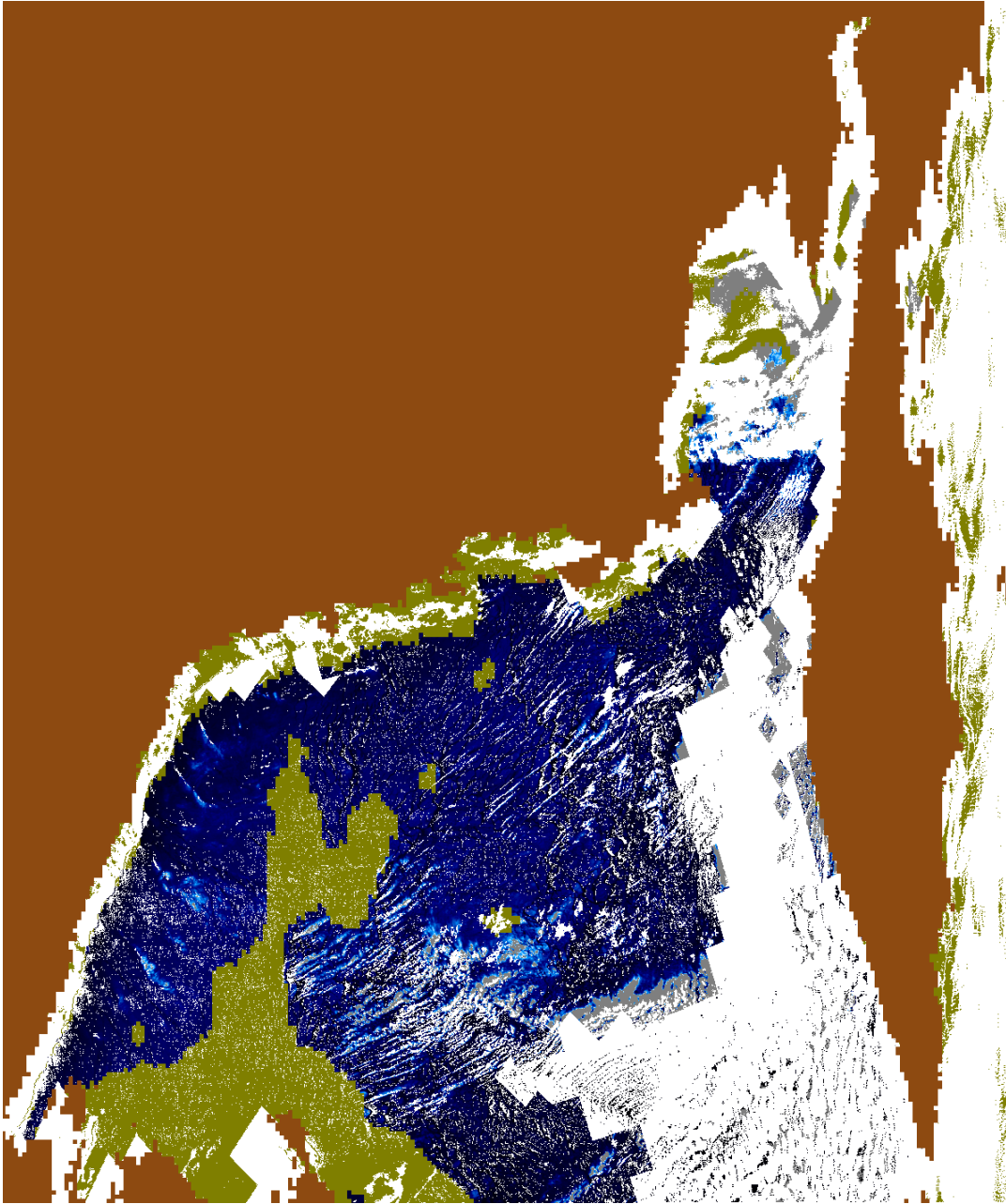
Figure 5.7: Sea of Okhotsk, February 27, 2009

In the figures 5.3-5.7 the Sea of Okhotsk is shown on different dates during the winter 2008-2009. Due to significant cloud cover it is difficult to follow the development of the ice in detail, but it is possible to get an impression. In the early data (figures 5.3 and 5.4) we see relatively small amounts of thin ice, and more grey in the north-western part of the sea, probably representing water (although we should keep in mind the limited cloud mask, see below). During the winter the north-western part of the sea gradually freezes over until it is all covered by ice (figures 5.5-5.7). This is in agreement with expectations and with other observations, for example Spreen et al. (2008).
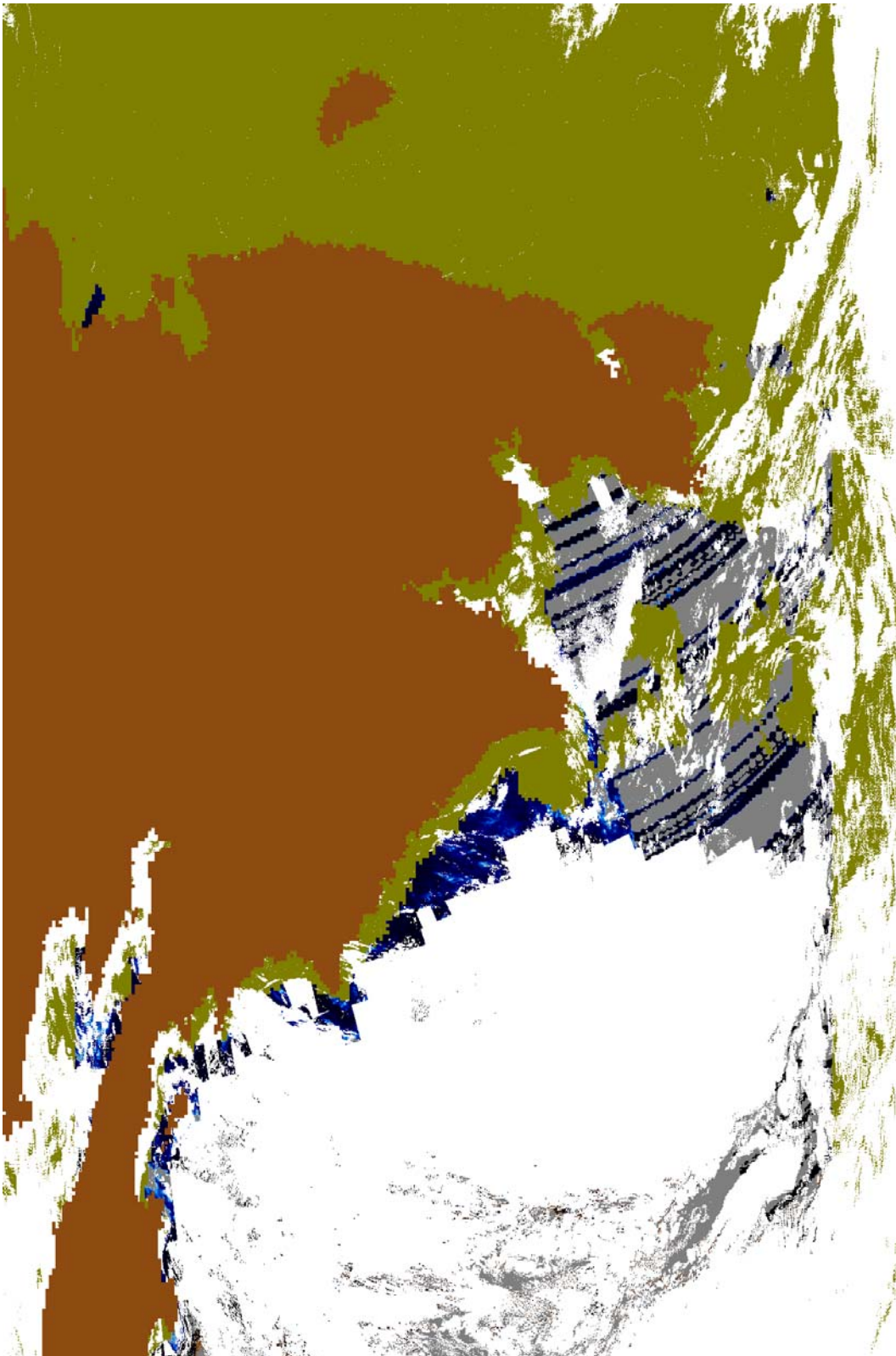
Figure 5.8: Bering Sea, January 26, 2009

Figure 5.8 shows the Arctic ice in the Chukchi Sea in the north masked out completely by the TIM. However, we also see some areas in the open sea which are masked out, although no ice is expected to be found there. There is also a peculiar striped pattern close to the Bering Strait. The origin of this pattern is still unclear.
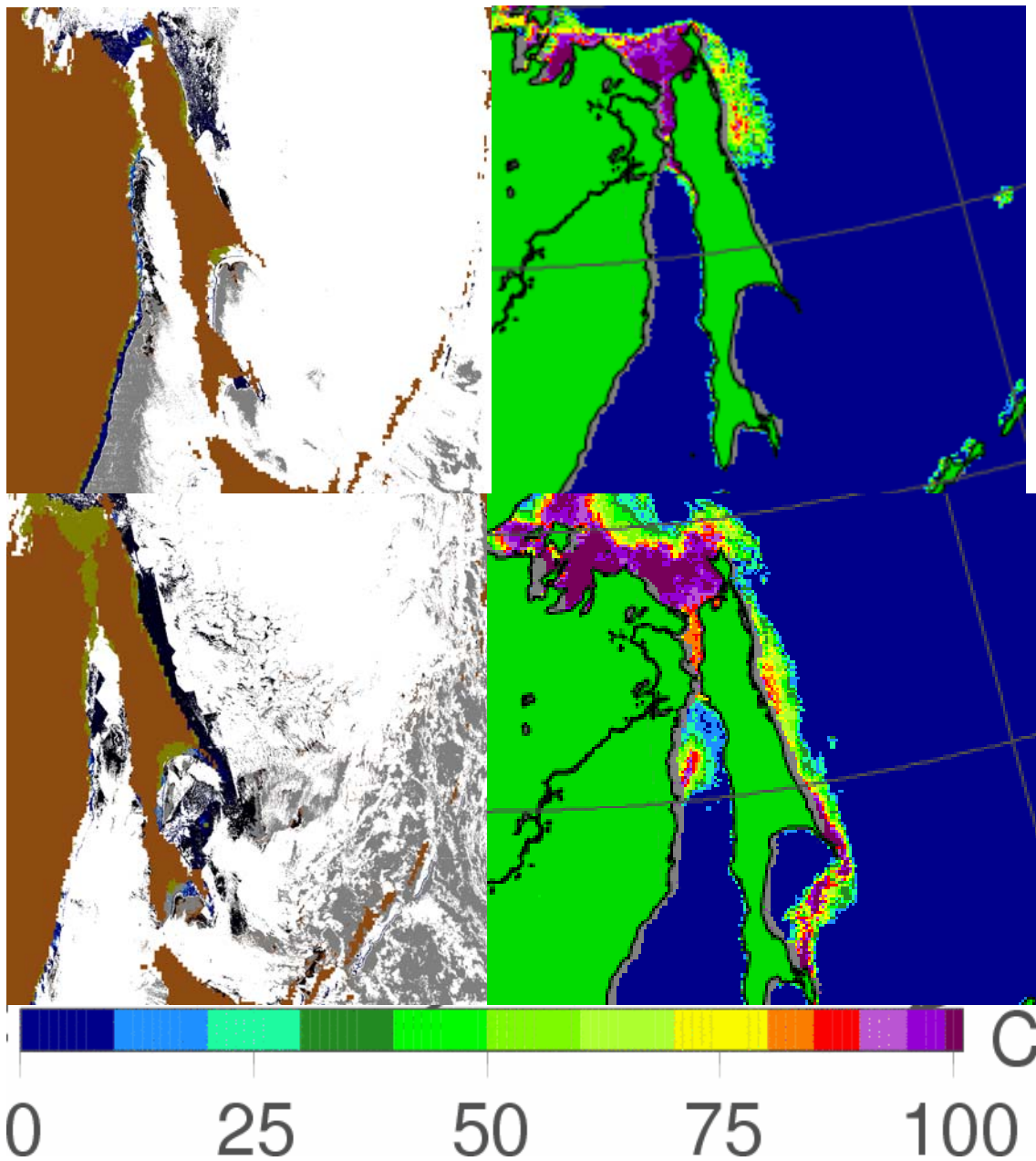
Figure 5.9: Sakhalin island on December 18 (upper) and January 12 (lower). The figures to the left show the ice extent as estimated by estimated by TTI and TIM, while the figures to the right show the ice concentration as estimated by Spreen et al. 2008. The legend shows the percentage of sea ice concentration. Note that the geometry is different between the images.
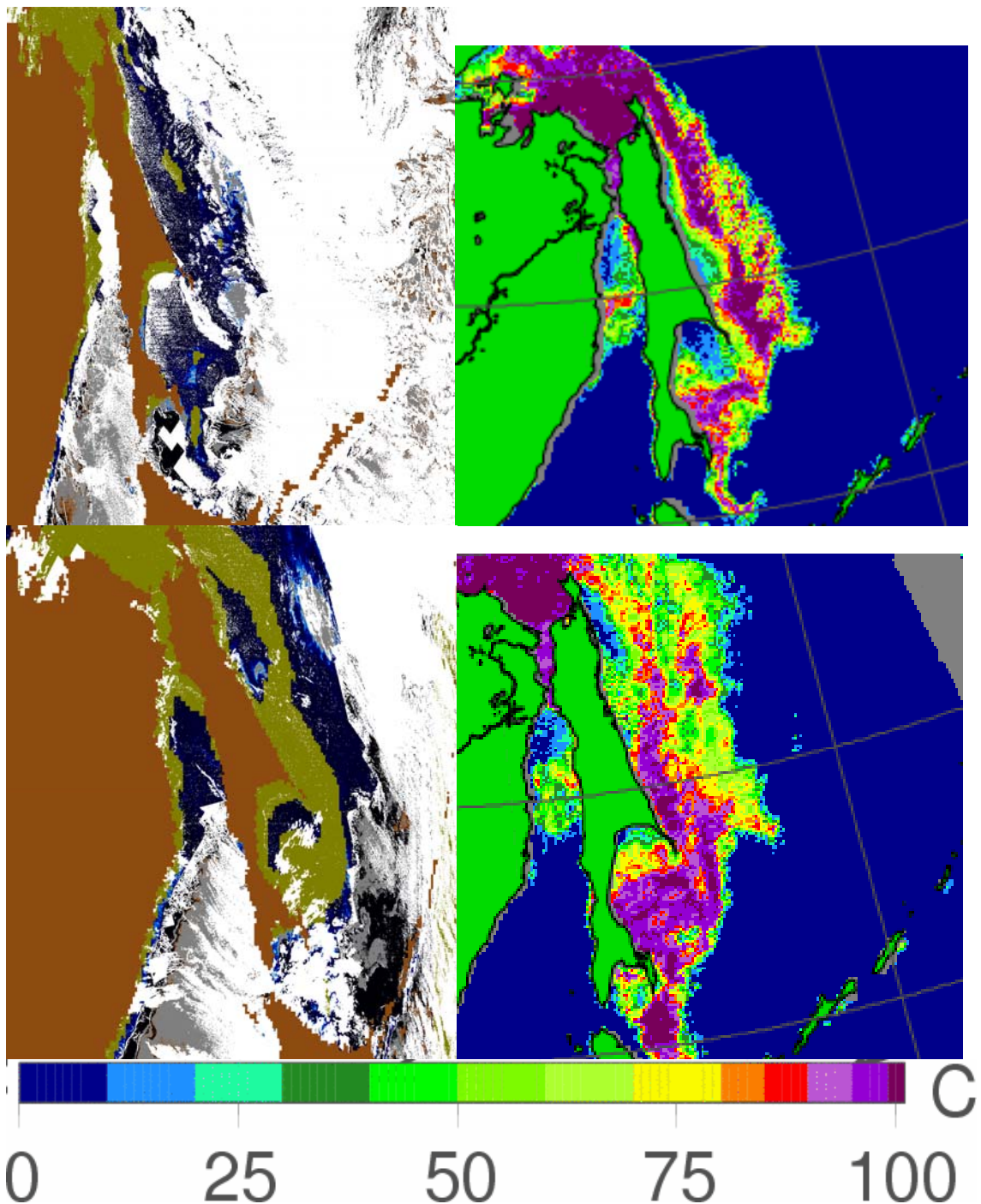
Figure 5.10: Sakhalin island on February 6 (upper) and February 25 (lower). The figures to the left show the ice extent as estimated by estimated by TTI and TIM, while the figures to the right show the ice concentration as estimated by Spreen et al. (2008). The legend shows the percentage of sea ice concentration. Note that the geometry is different between the images.

In figure 5.9 and 5.10 the island Sakhalin in the Sea of Okhotsk is shown on different days throughout the winter. We clearly see the extent of sea ice increasing through the winter, as is expected, from almost nothing in December, and reaching a large extent in the end of February. For comparison the ice concentration maps for the same area, prepared by The University of Bremen (Spreen et al. 2008) are shown in the right column in the figures. As seen from these images there is a general agreement between the ice extents in these estimates.

5.1.2 The cloud mask

The most obvious challenge is cloud masking. The cloud mask contains a significant amount of clouds, and knowing which pixels contain reliable information is essential. The current cloud mask does not capture all clouds, and results in pixels with incorrect estimates of ice content and thickness. In figure 5.11 we see how some areas with non-detection (grey areas) contain a "halo" of estimated thick ice. When inspecting the original thermal data we see that this is likely clouds that have not been properly removed by the cloud masking.
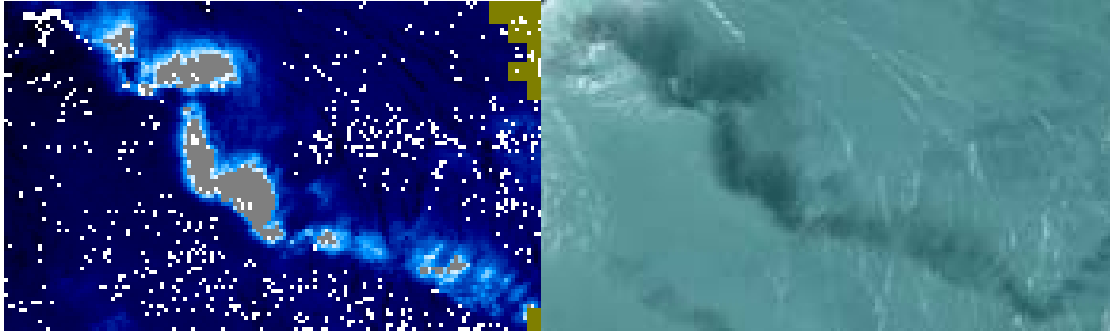

Figure 5.11: Detection of thick ice, or water (left) is more probably clouds when investigating infrared data (right). Note the "halo" of estimated thick ice around the grey areas.

This limitation is quite significant, since much of the unmasked results are near clouds, and an unreliable cloud mask leads to uncertainty of the correctness of the thin ice estimates. Figures 5.12-5.14 demonstrates how an unreliable cloud mask reduces the quality of the output.
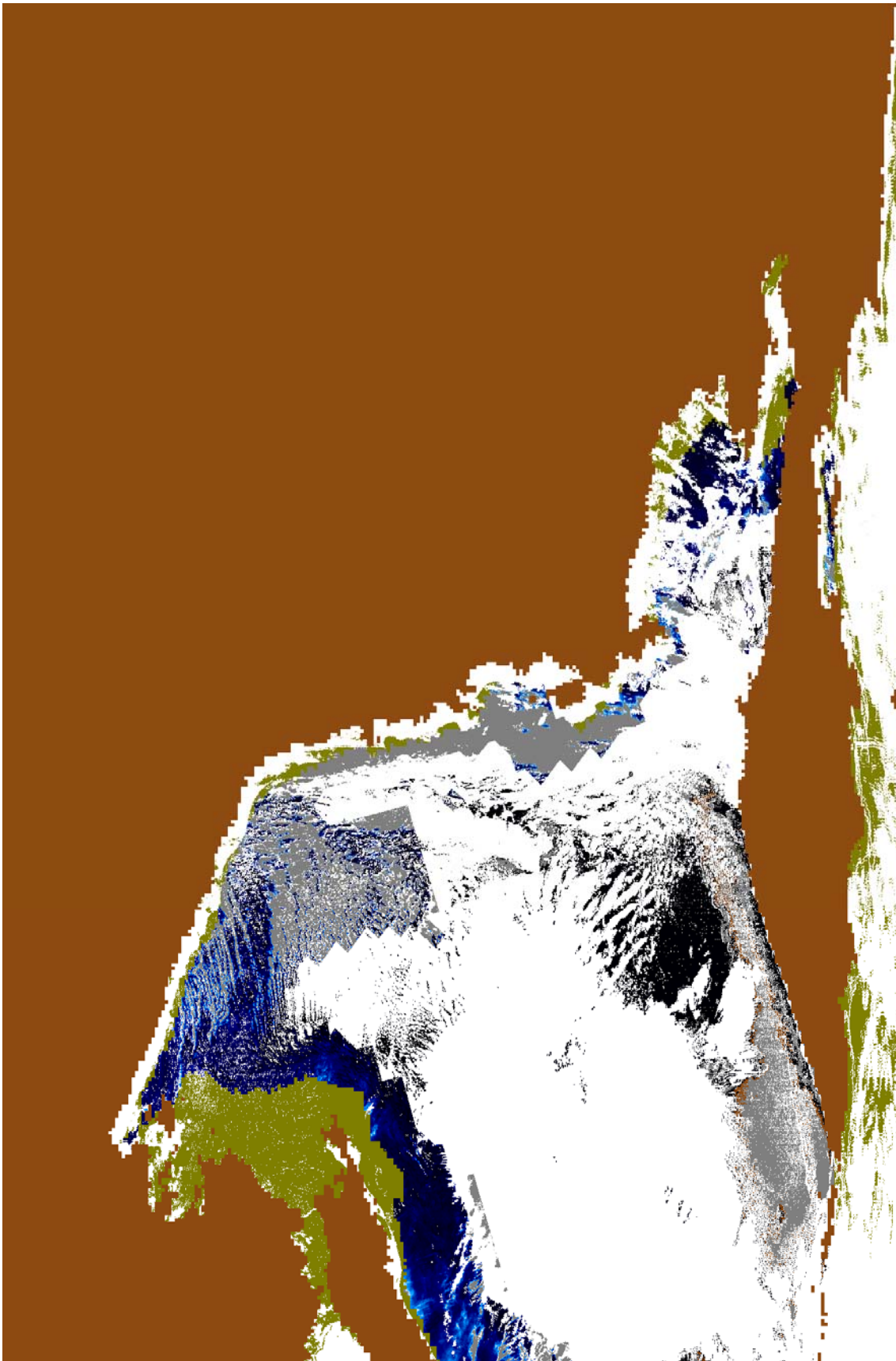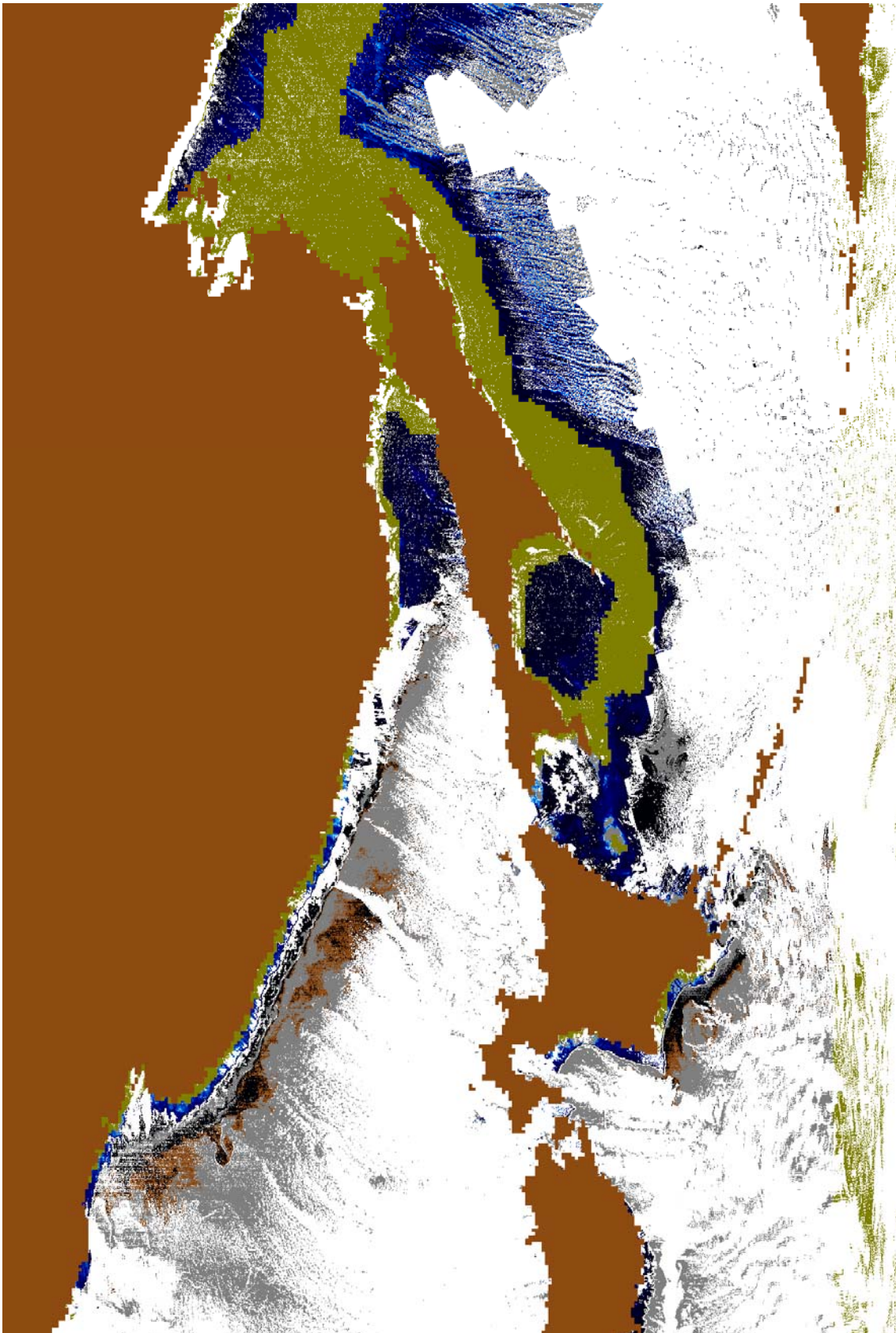
Figure 5.12: Sea of Okhotsk, January 26, 2009

NR🌐 *ThinIce* **D1, D2, D3 - Retrieval of thin sea ice thickness from thermal optical data**

Figure 5.13: Sea of Okhotsk, February 18, 2009
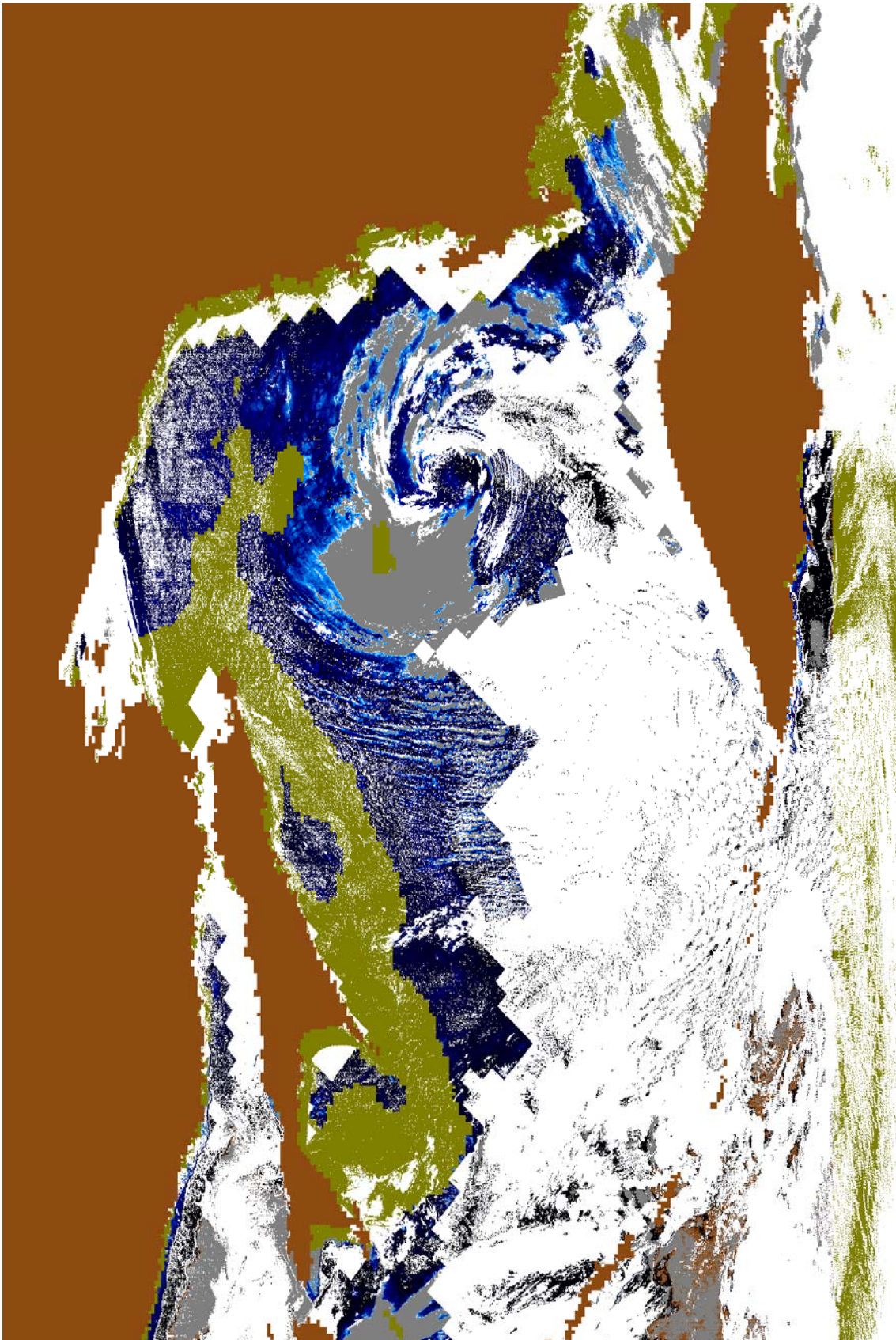
Figure 5.14: Sea of Okhotsk, March 1, 2009

NR🌐 *ThinIce* **D1, D2, D3 - Retrieval of thin sea ice thickness from thermal optical data**

In figure 5.12 unmasked clouds are clearly influencing the mask. It is hard to interpret the scattered area in the centre, containing ice, clouds and grey. Figure 5.13 shows a similar situation. Here it is difficult to estimate the extent of the ice in the region along the edge of the clouds. Figure 5.14 shows a storm in the sea of Okhotsk. Here there are obviously unmasked clouds influencing the results, since we have a large, spiral pattern of grey, surrounded by a halo of light blue. Also note the TIM mask in the grey area, indicating an area of old ice within the storm.

We see from these results that an improved cloud masking algorithm would significantly improve the quality of the results.

5.1.3   TIM and TTI

As seen from the images above the TTI algorithm is capable of detecting the extent of thin ice. The estimated thin ice shows a steadily growing ice coverage which agrees with other observations. We also see that the TIM grows throughout the winter as the ice becomes "old".

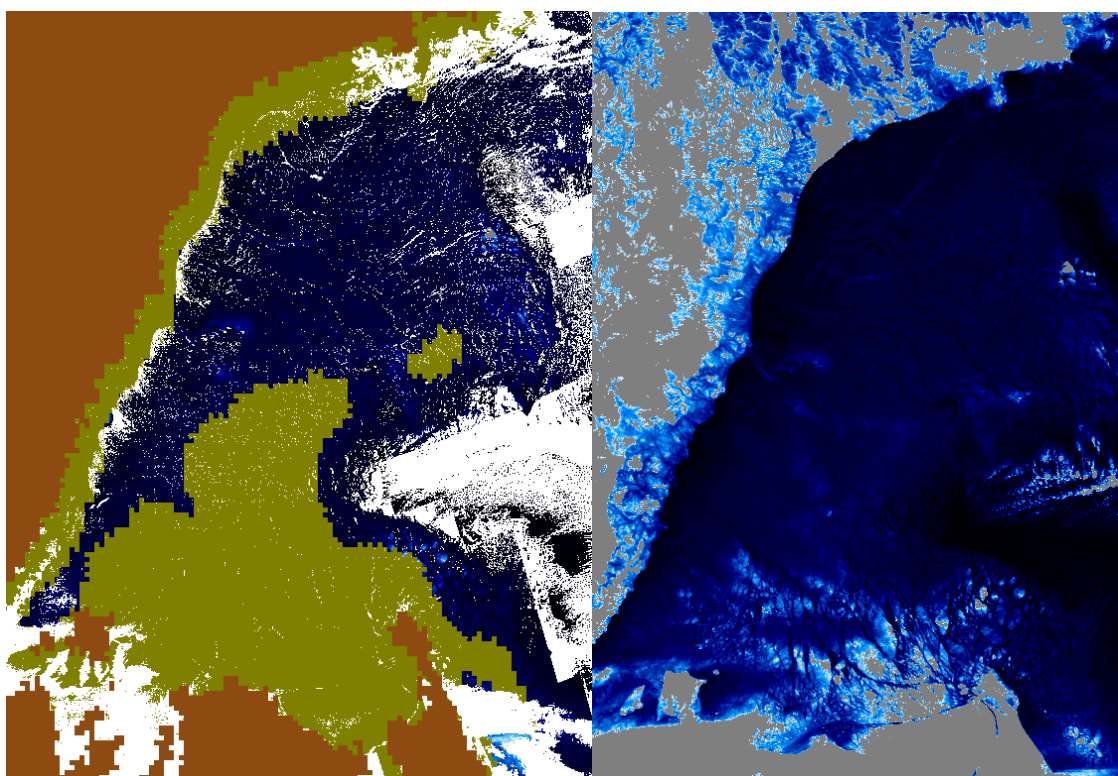Figure 5.15 shows the Russian coast by the Sea of Okhotsk, with and without TIM.

Figure 5.15: The Russian coast by the sea of Okhotsk January 1, 2009, with TIM (left) and without (right). Note that the right image does also not have land or cloud masks.

This figure shows an open area, relatively free from clouds. Note that in the left image TIM masks out areas in the south and along the coast in the west. In the right image we see that the same areas are estimated to contain thick ice by TTI. That the two independent algorithms based on two different data sets show agreement, is promising.

It is still unclear exactly what the TIM is sensitive to. According to the empirical model described in section 2.2, it masks areas with *first year ice*, but not with *new ice*. Whether the distinction between these two types of ice is due to thickness, age or other factors, is not yet

clear. From the data (for example figure 5.8) the TIM also masks out certain areas in the middle of the open sea, where it is unlikely to exist sea ice. Some more tests are needed to properly understand this mask.

5.2 Daytime images

Figures 5.16-5.21 show results from daytime images when accounting for the solar radiation heat flux. All the images are taken from the Sea of Okhotsk. The colour mapping is the same as for the night images.
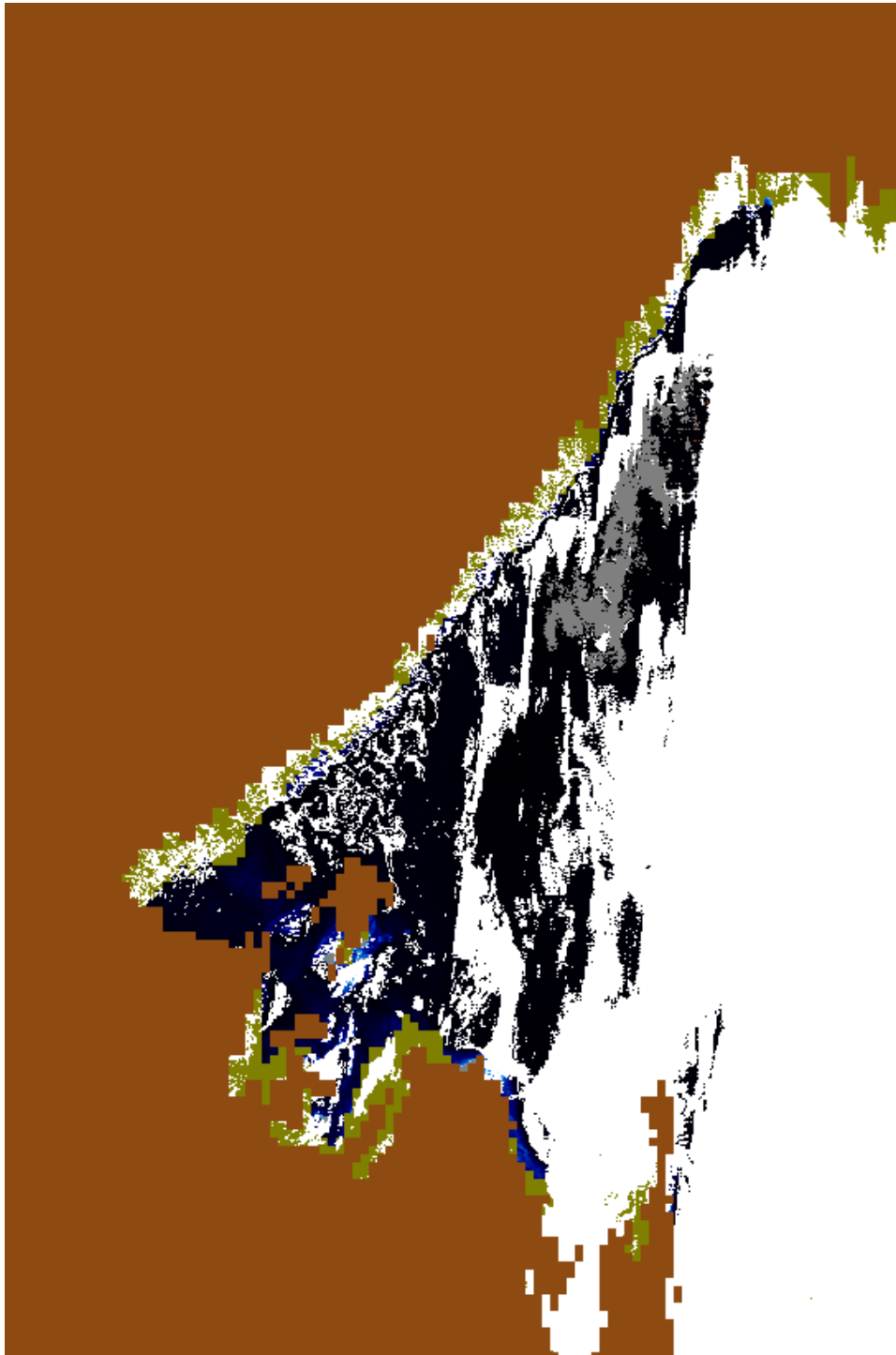

Figure 5.16: Sea of Okhotsk, January 2, 2009

Again, we see relatively small amounts of thin ice in the early January (figure 5.16) and later the extent and thickness of the ice grows (figure 5.17 and 5.18). This agrees well with the corresponding results for the night images (figure 5.4 and 5.5).

The cloud mask certainly performs better in the case of daytime images. The halo effect, with estimated thicker ice along the edges of the clouds has almost vanished. Figure 5.19 shows a storm in the Sea of Okhotsk. Some possible pollution of the thin ice estimates can be seen. However, when comparing to a similar scenario for the night images (figure 5.14) it is clear that the daytime cloud mask is a significant improvement from the cloud mask of the night images.

For the daytime another problem is visible. In the later images (figure 5.20 and 5.22), when the ice grows thicker, the algorithm breaks down. This is seen as grey areas in the maps. It appears that the ice thickness is estimated too high, and sometimes this causes the estimate to fall in another ice thickness regime, used for estimating salinity, snow thickness, albedo and transmittance (see eqs. 3, 4 and 6 in section 2). When the error becomes too large, no valid solution is found. The effect is correlated with crack-like structures in the ice (figure 5.21).
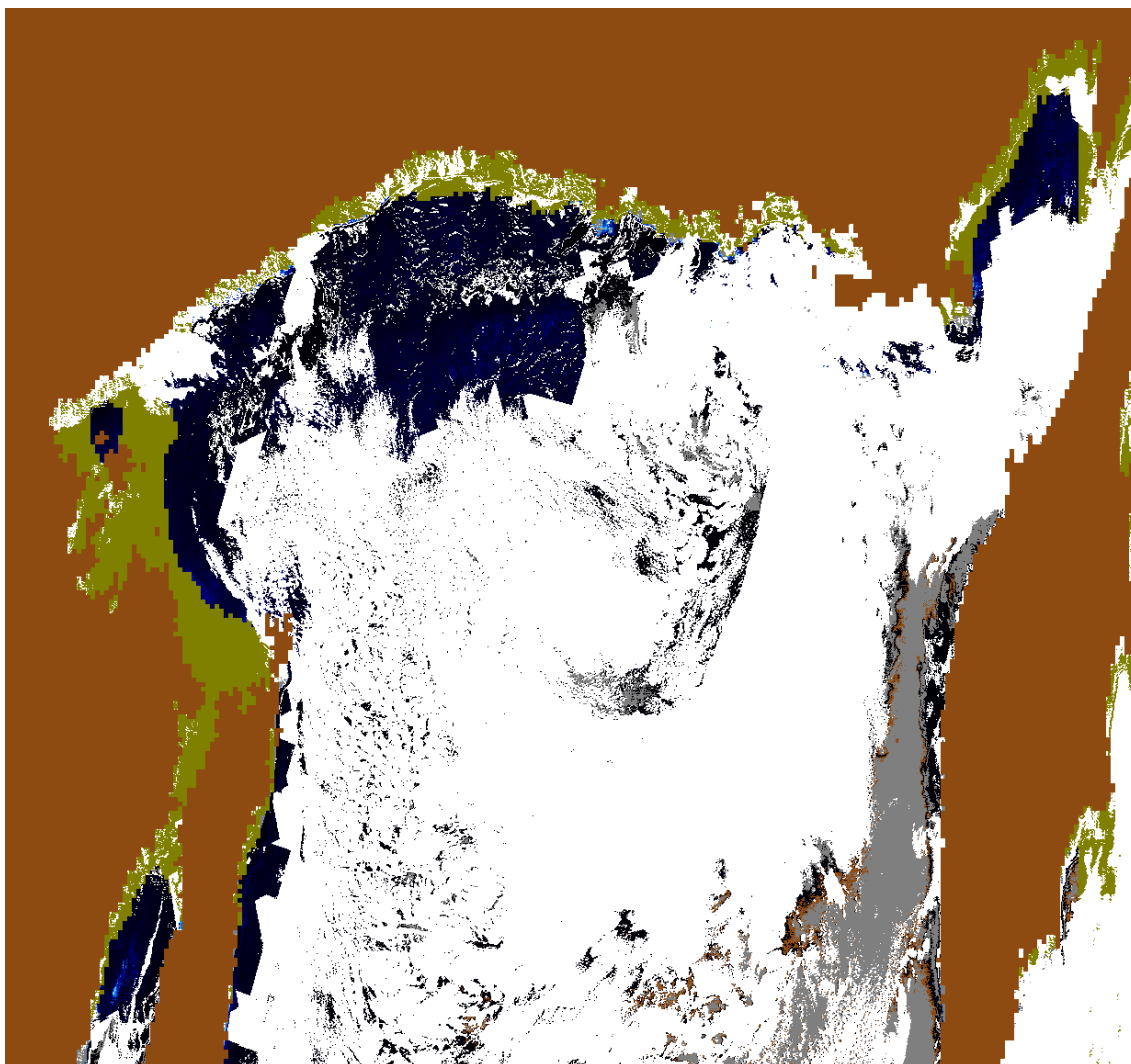

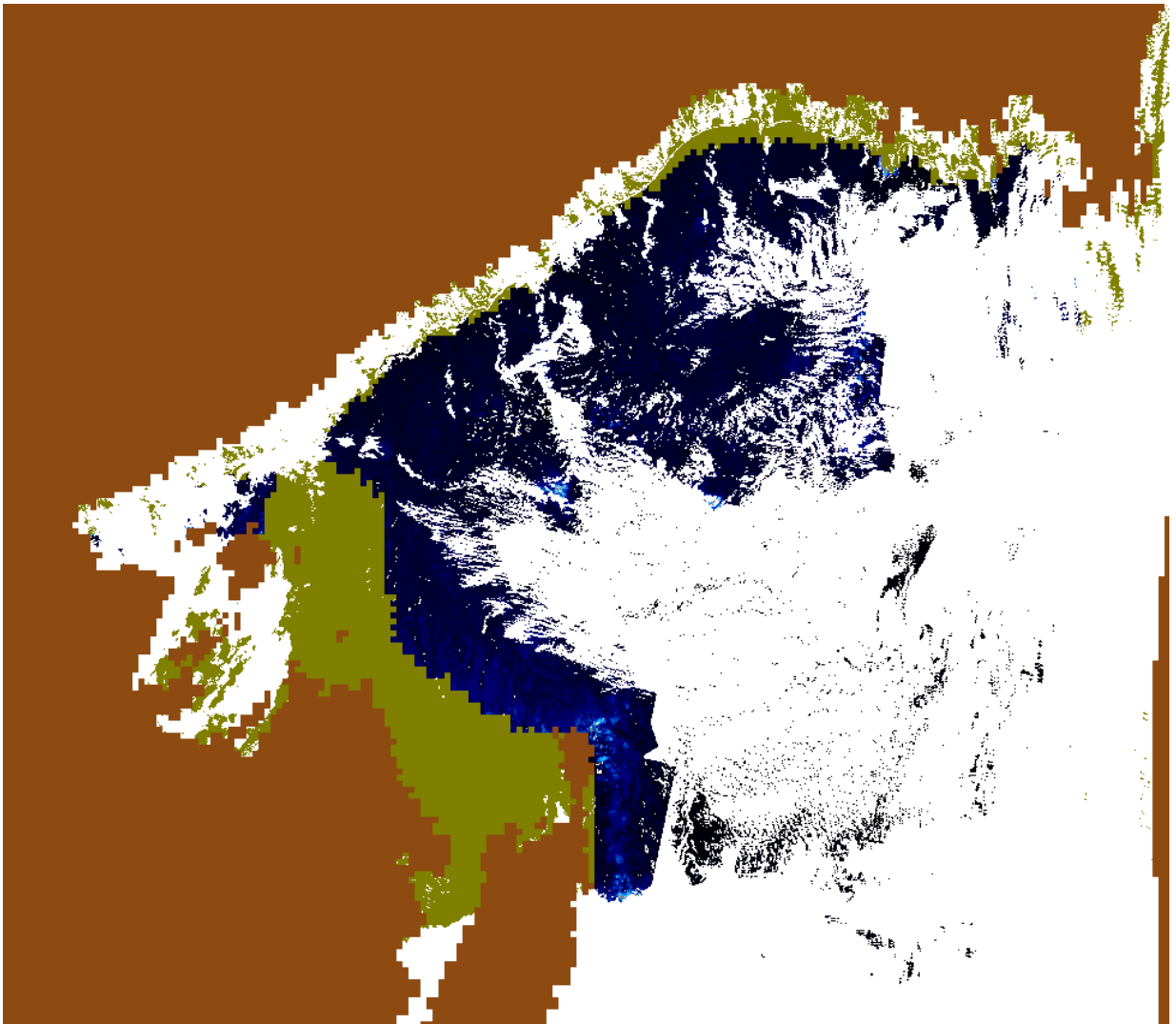
Figure 5.17: Sea of Okhotsk, January 12, 2009

Figure 5.18: Sea of Okhotsk, January 15, 2009

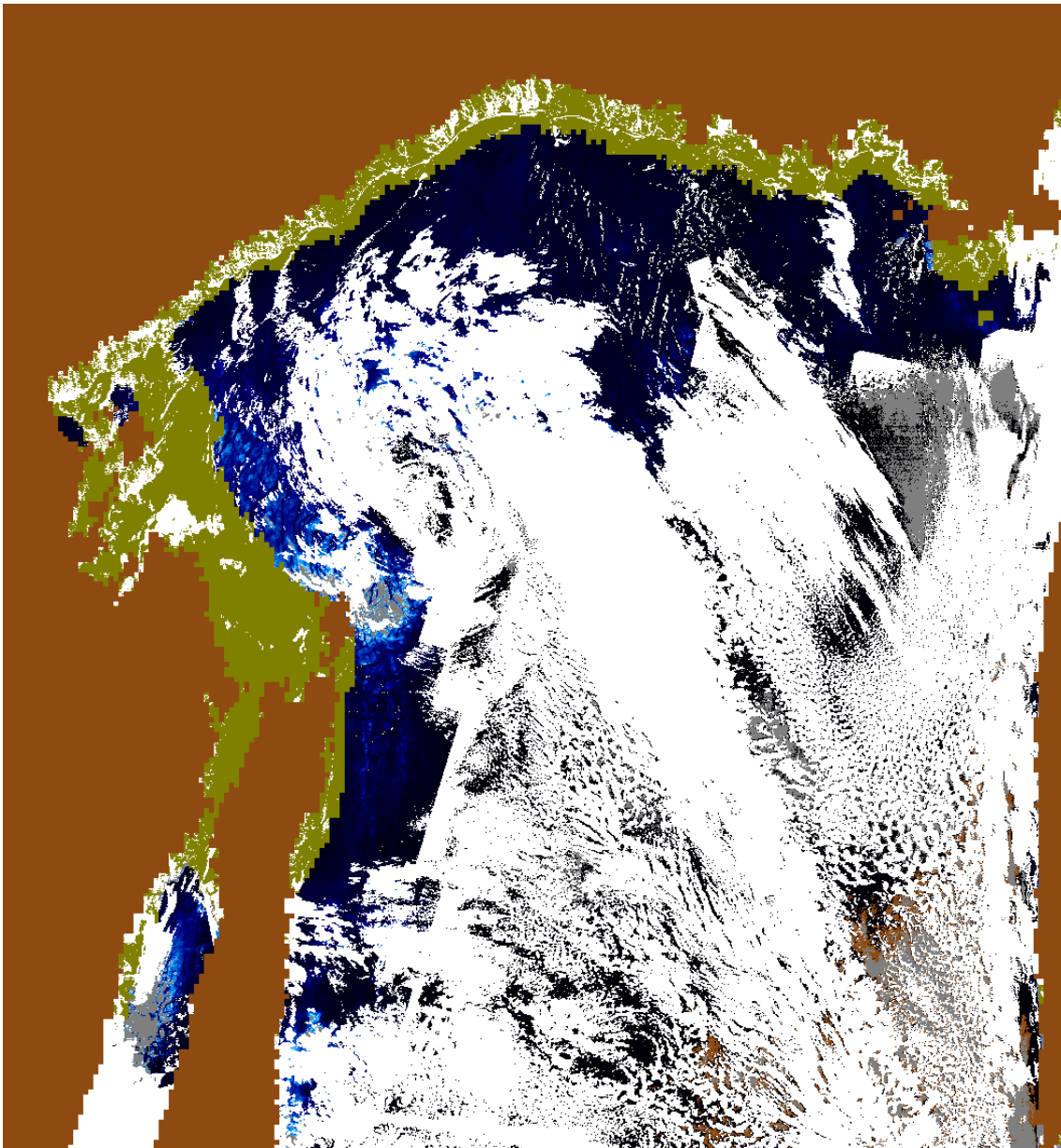NR *ThinIce* **D1, D2, D3 - Retrieval of thin sea ice thickness from thermal optical data**
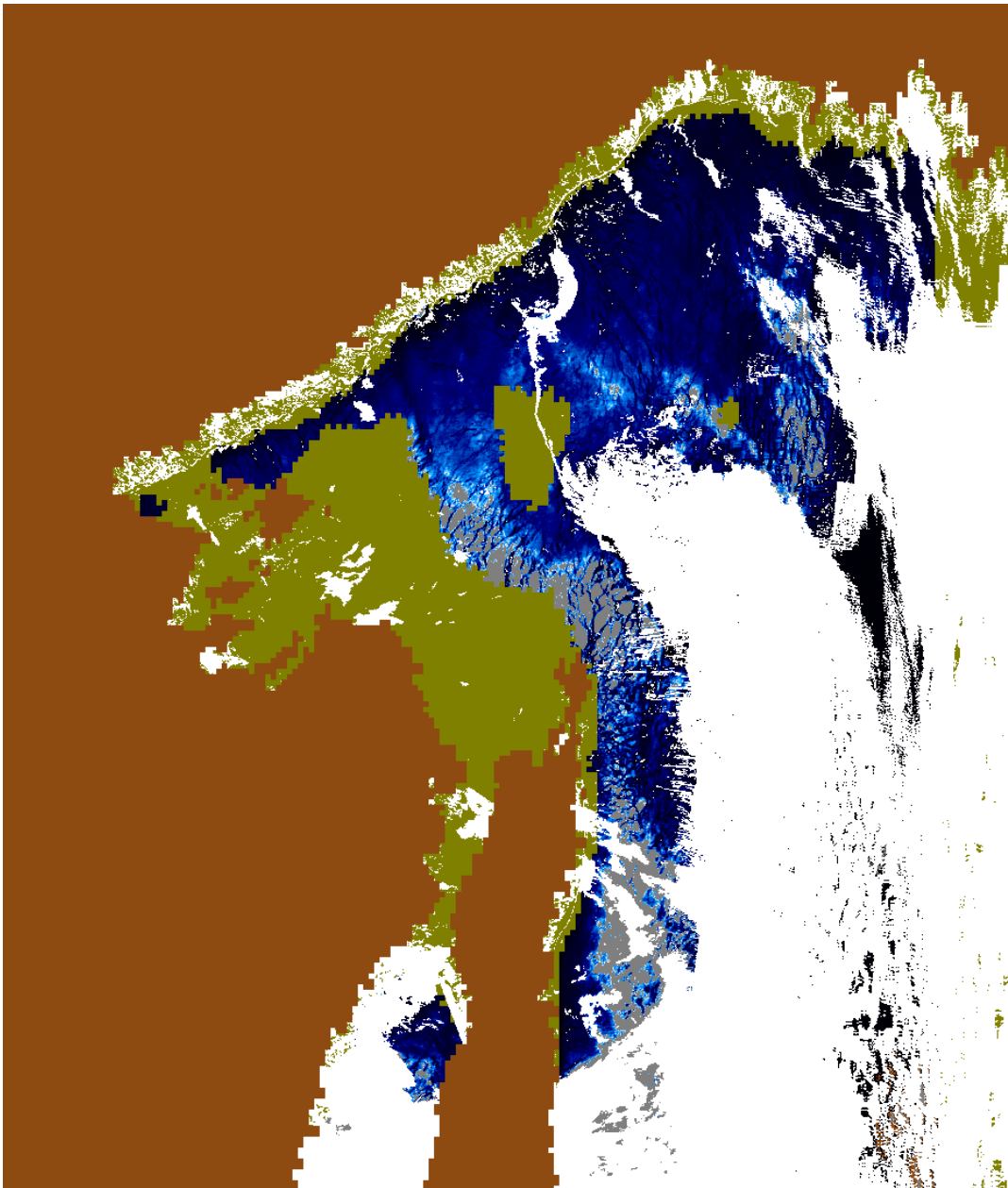
Figure 5.19: Sea of Okhotsk, January 19, 2009
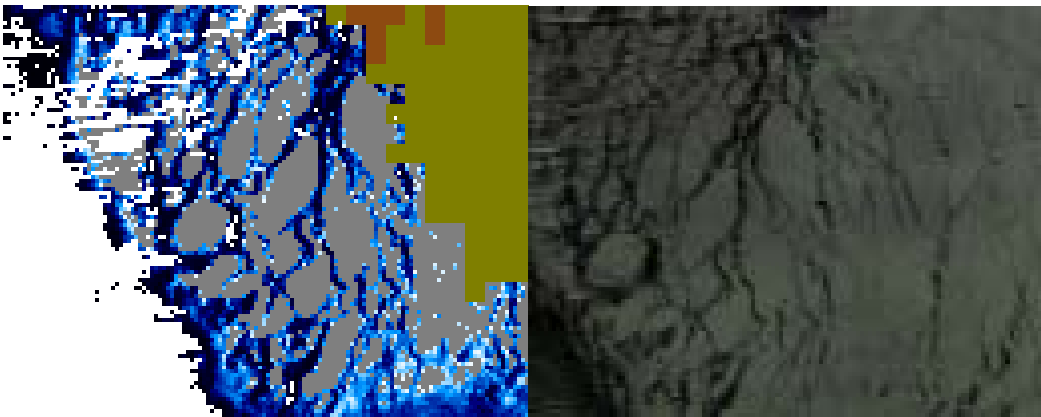
Figure 5.20: Sea of Okhotsk, January 22, 2009

Figure 5.21: Sea of Okhotsk, January 22, 2009. Thin ice thickness (left) and false colour optical image (right). Areas where the algorithm breaks down, corresponds with crack-like structures in the ice.
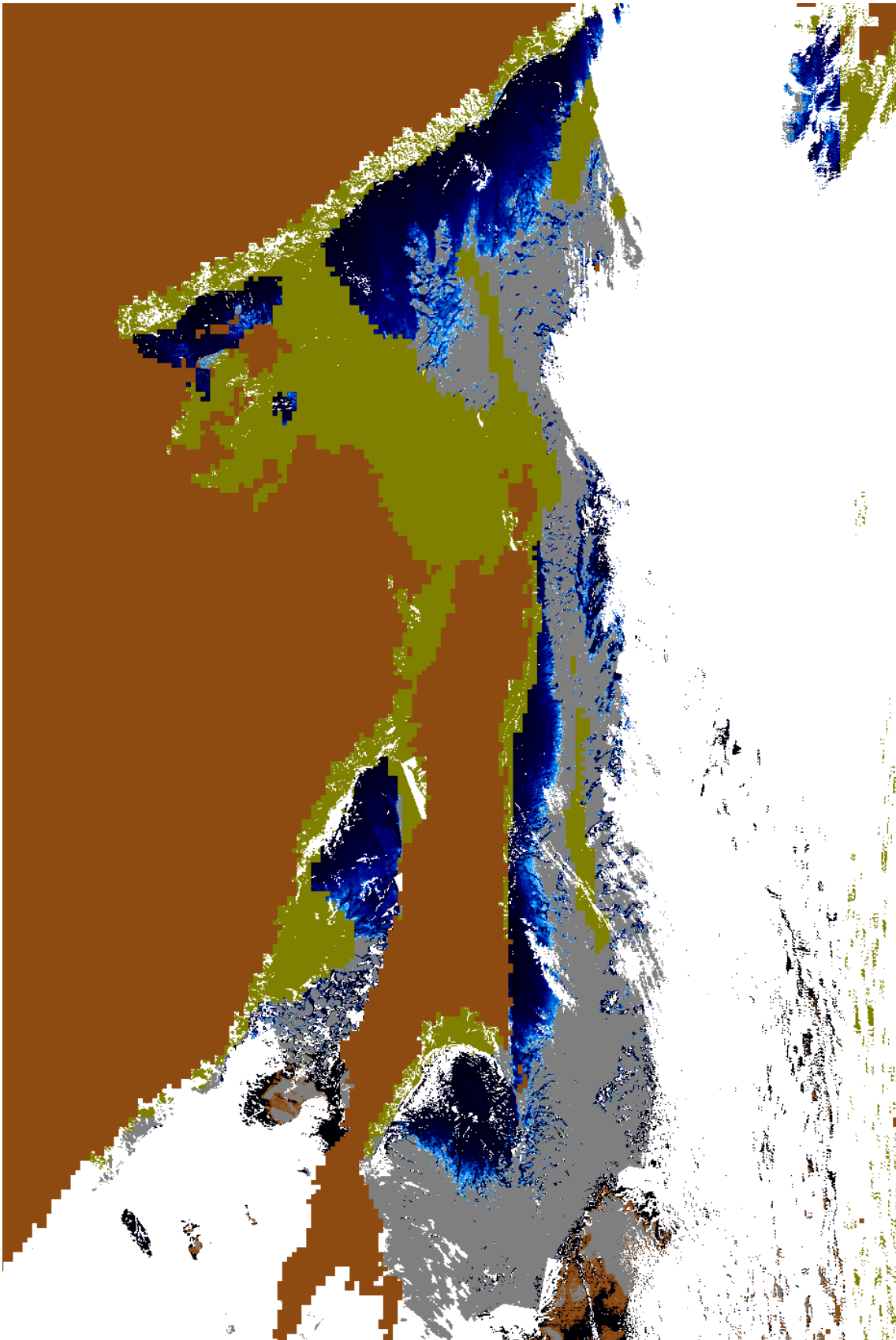
NR◉ *ThinIce* **D1, D2, D3 - Retrieval of thin sea ice thickness from thermal optical data**

Figure 5.22: Sea of Okhotsk, February 7, 2009

6 Evaluation

The results from Laptev Sea generally contain a large amount of clouds. Nevertheless, we will attempt to get a general understanding of the sea ice coverage in the area by studying the unclouded pixels in the results.

6.1 Night images

From figure 6.1 we see that most areas around the coast are ice covered, often with thick ice. A large thick ice sheet is visible in the north-west. The parts of the ice sheet which are not covered by the thick ice mask and not obviously polluted by unmasked clouds, are estimated to be 15-30 cm thick. The central Laptev Sea contains open water or very thin ice (< 1 cm).
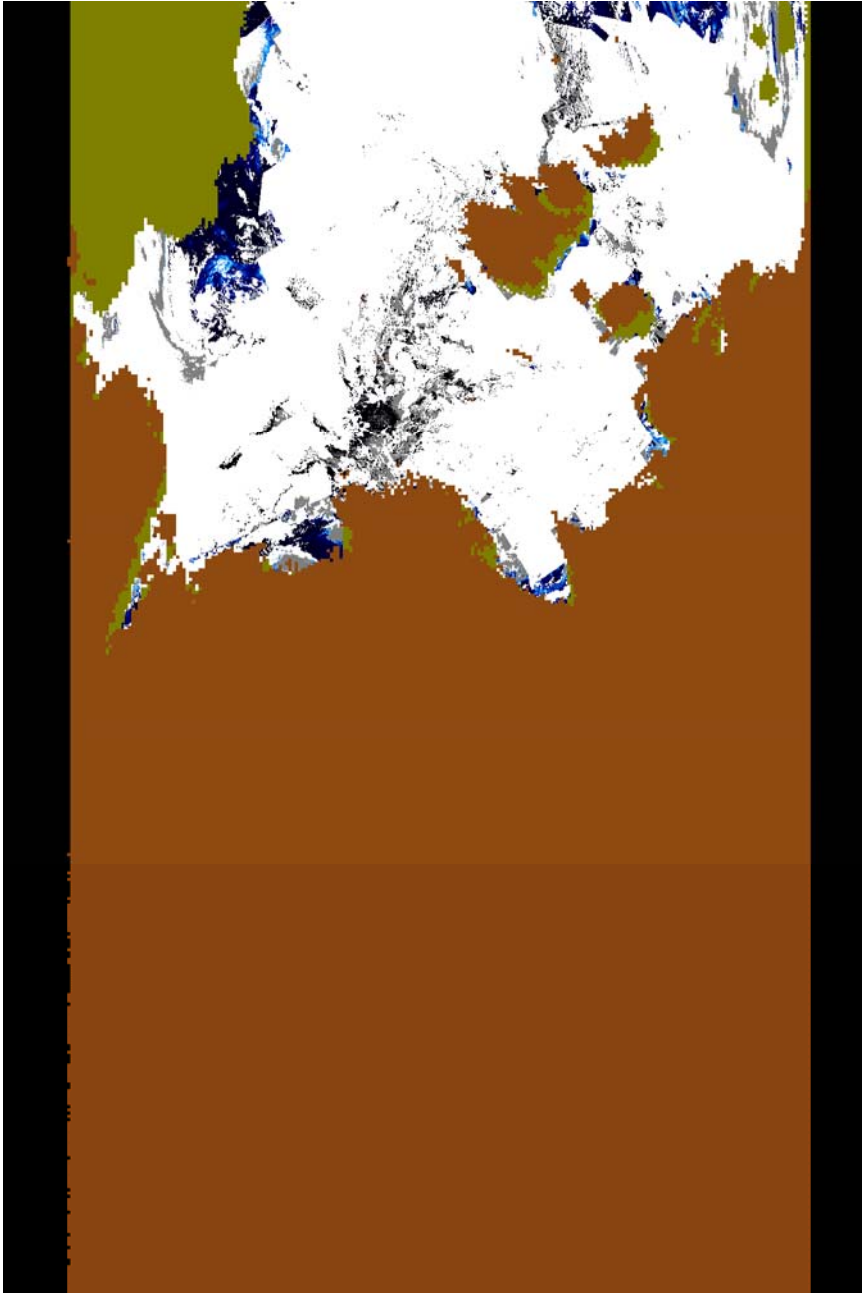

Figure 6.1: Laptev sea, October 13, 2010

In figure 6.2 we see some artefacts in the north-western corner of the image. This probably originates from the resampling and reflects problems with the coordinates in the northernmost areas.

The image shows a large, thick ice sheet stretching from the Arctic to the Russian coast. The areas immediately close to the thick ice mask indicate open water, while a sheet of thin ice is shown closer to the coast. The part of the thin ice close to the coast, and in the centre of the Laptev Sea, are estimated to 0-5 cm thick, while the part closer to the thick ice sheet is shown to be 5-15 cm thick.
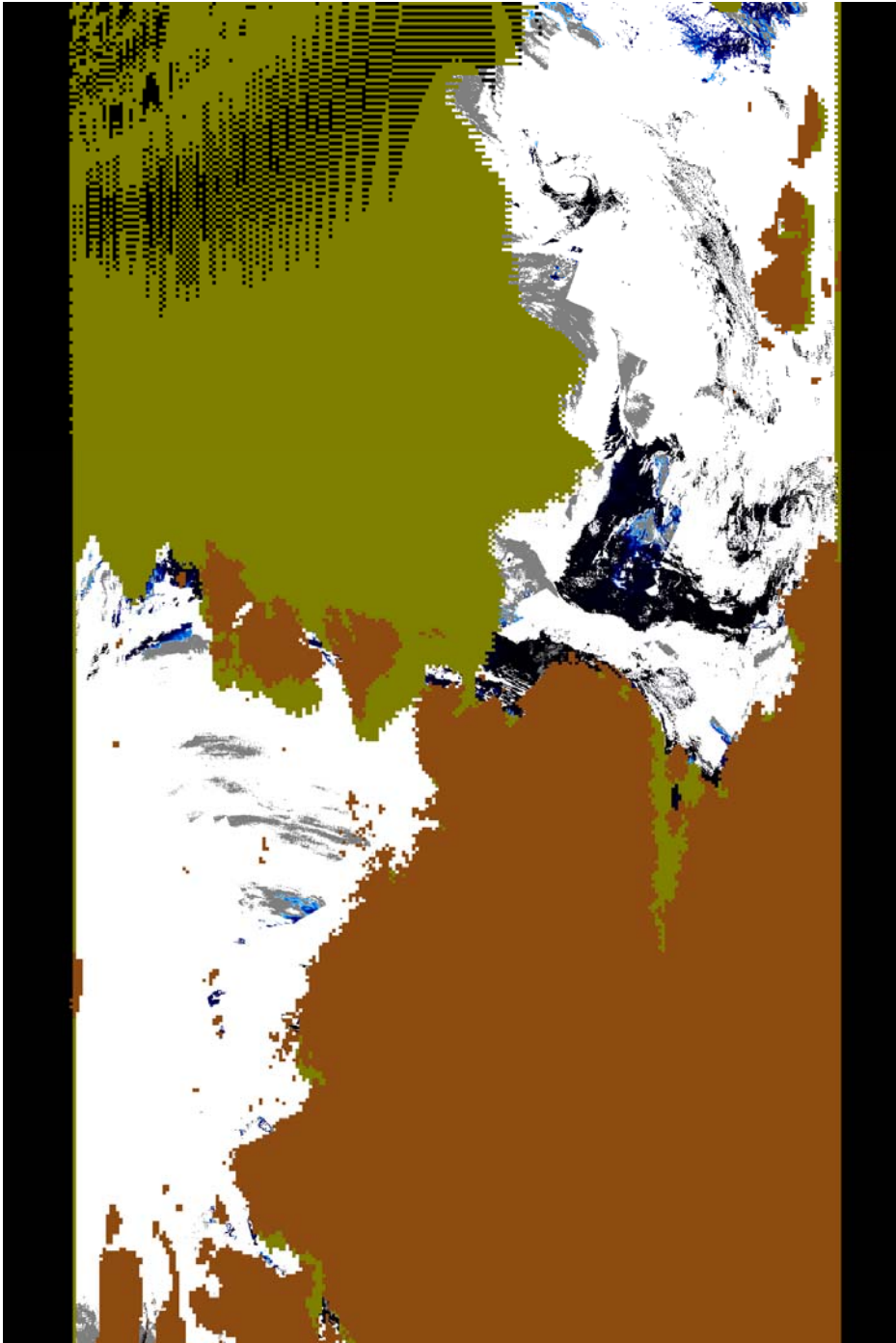
Figure 6.2: Laptev sea, October 14, 2010

In figure 6.3 the coordinate artefacts are again seen in the northern parts of the image. The rest of the image shows a large Artic ice sheet in the north, with two tongues stretching towards the Russian coastline. Thin sea ice is seen by the tip of the eastern part of the ice sheet (15-30 cm thick), between the western part of the ice sheet and the coast (5-15 cm thick) and north of the central islands (0-1 cm thick). Several grey areas indicate that most of the remaining part of the Laptev Sea contains open water.
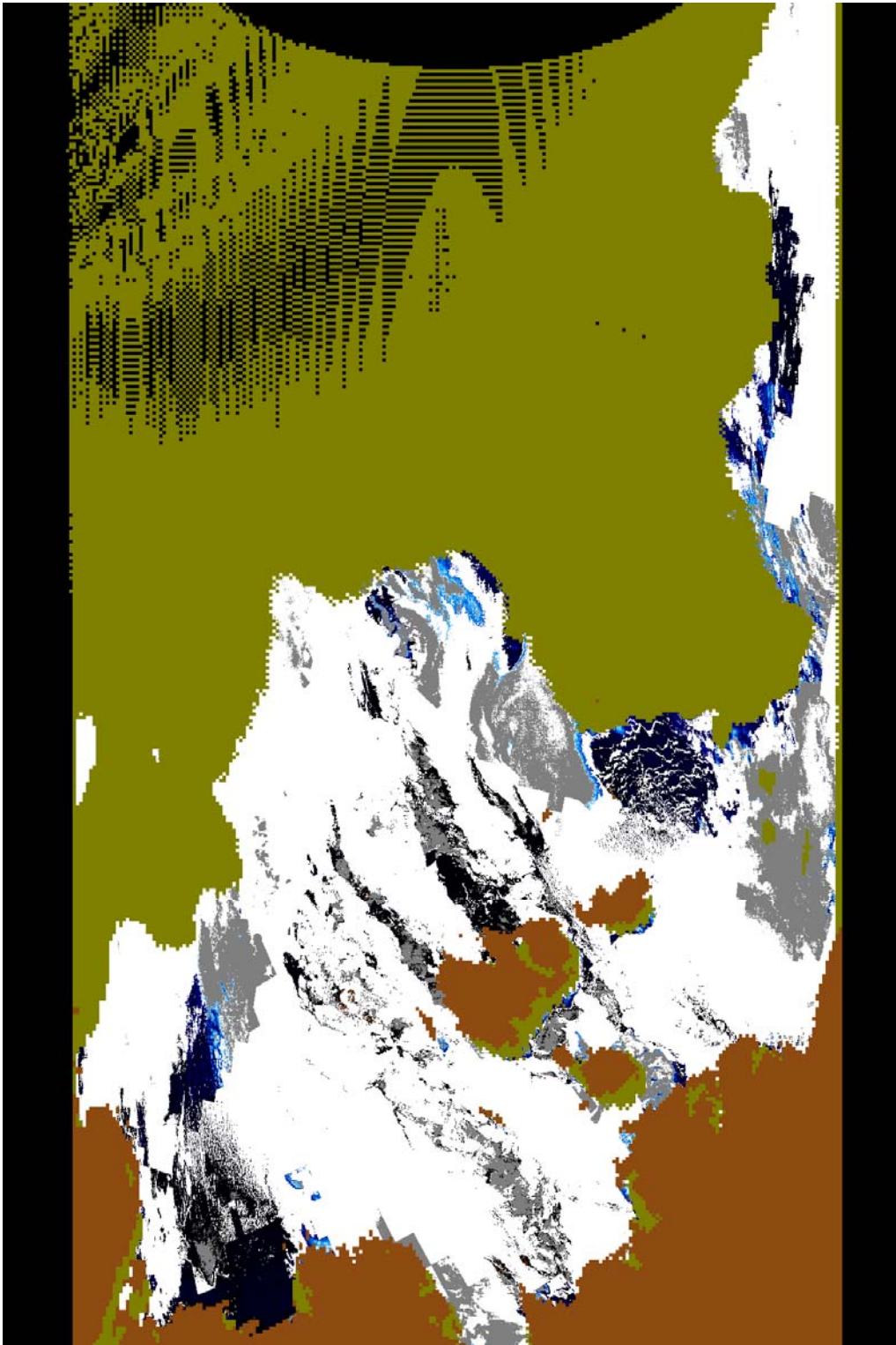
Figure 6.3: Laptev sea, October 15, 2010

6.2 Daytime images

In the unclouded pixels of figure 6.4 we see thin ice along the Arctic ice sheet, with thickness up to 25 cm. The ice seen in the central parts of the Laptev Sea is estimated to be 0-5 cm thick.
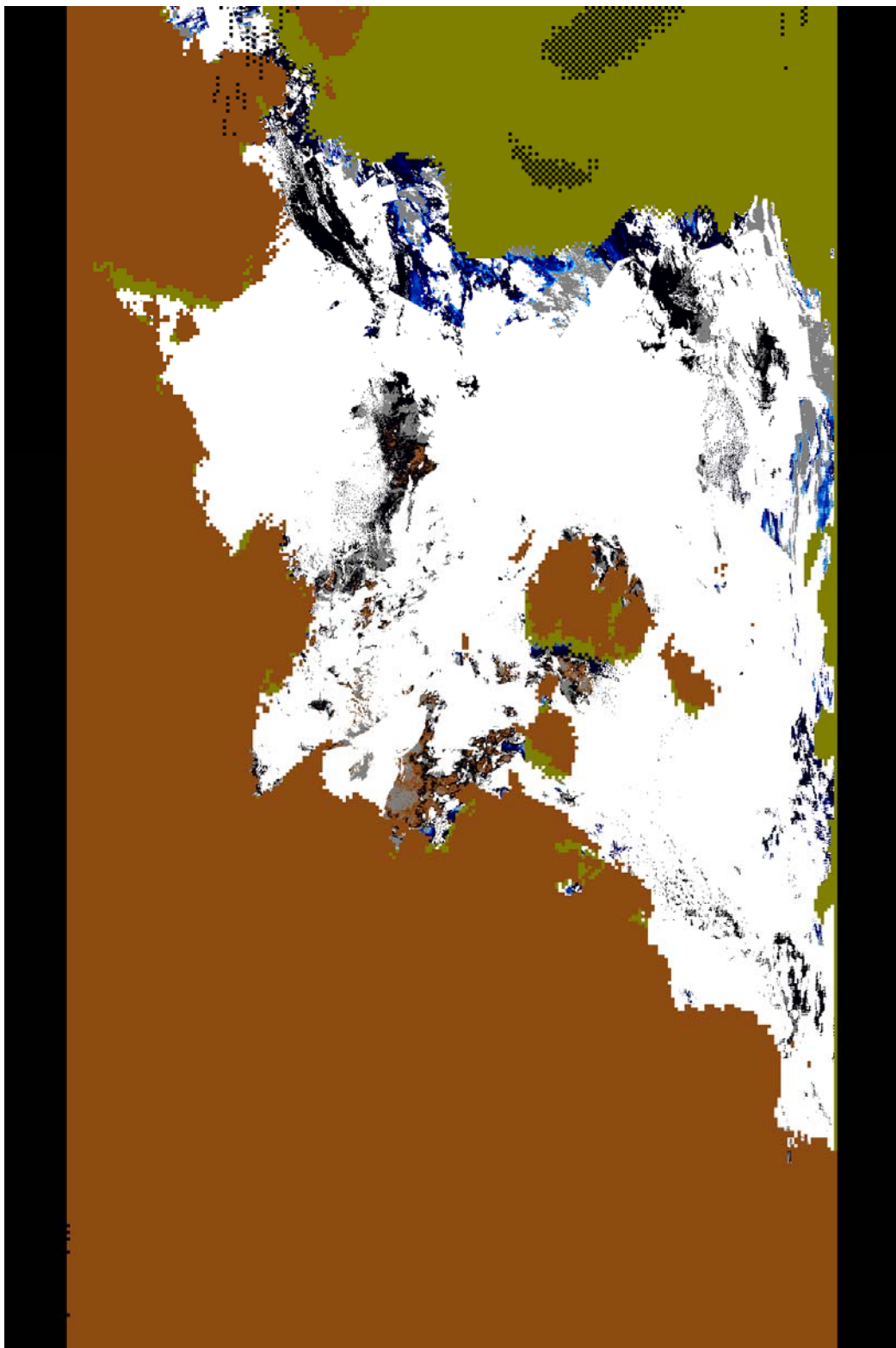
Figure 6.4: Laptev sea, October 11, 2010

In figure 6.5 no ice is seen close to the Arctic ice sheet. Some ice is detected further south, however, with an estimated thickness of 15-25 cm. Even further south, in the few unclouded pixels we see open water and small patches of thin ice with thickness 0-5 cm.

Figure 6.5: Laptev sea, October 14, 2010

NR *ThinIce* **D1, D2, D3 - Retrieval of thin sea ice thickness from thermal optical data**

In the final daytime image, figure 6.6 we see once more a patch of thin ice (5-20 cm thick) by the end of the thick Arctic ice sheet in the north. In the east we also see an estimate of relatively thick ice (up to 1.5 m), thicker than the range of validity of our model. This effect is likely the result of unmasked clouds.

Figure 6.6: Laptev sea, October 15, 2010

6.3 Comparison with ice thickness from SMOS

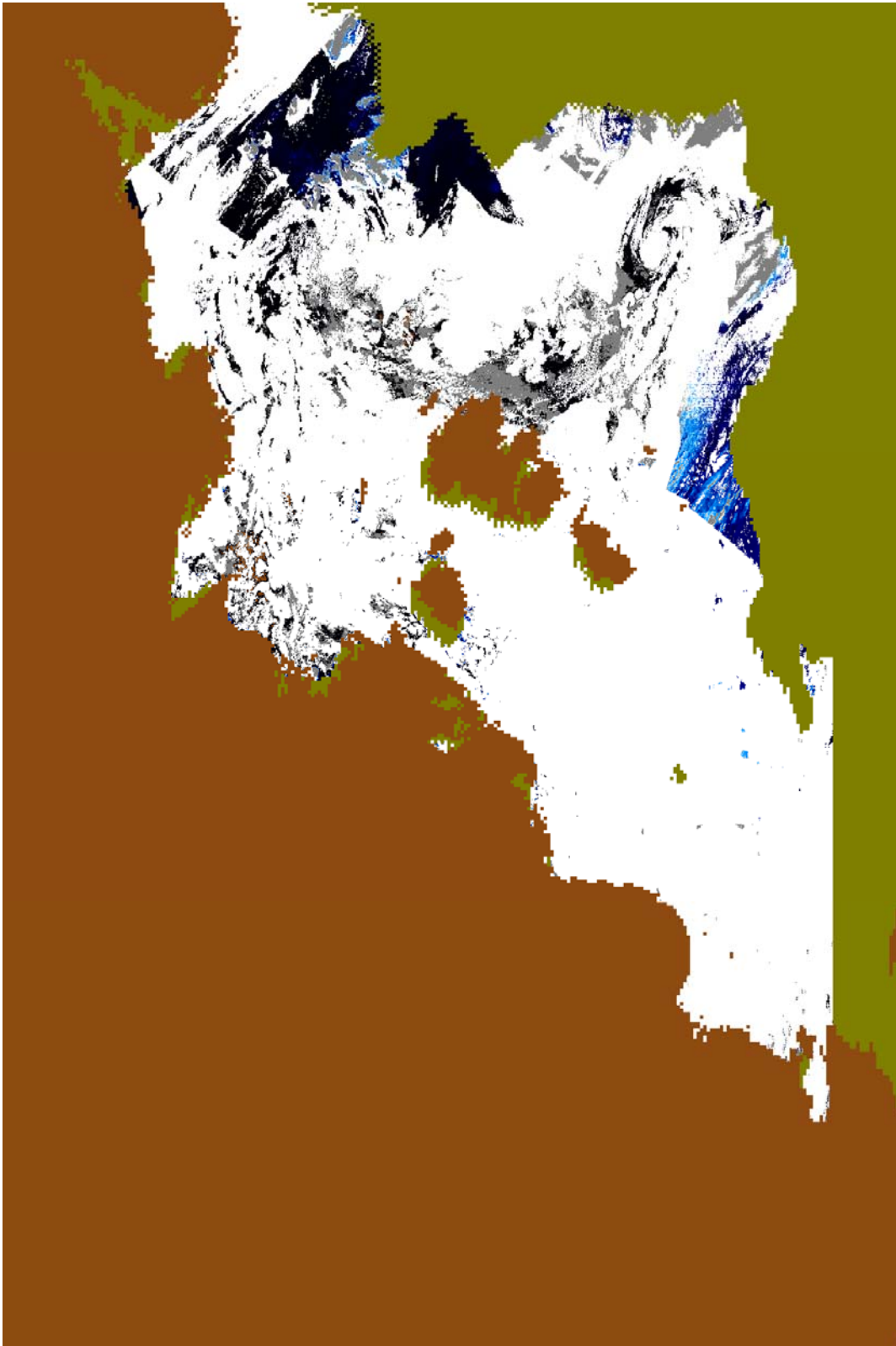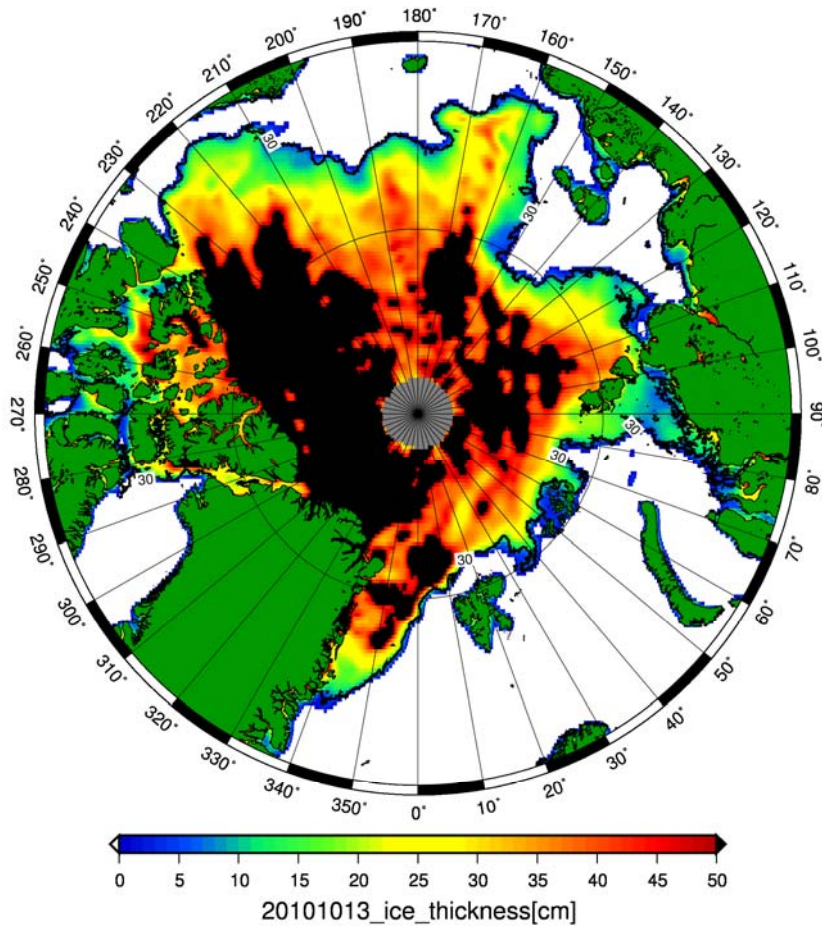Figure 6.7: Thin ice thickness estimate with SMOS, October 13, 2010. (Wang & Heygster, 2011)

The thin ice estimate from SMOS (figures 6.7 and 6.8) shows a similar general situation (Wang & Heygster, 2011). In figure 6.8 we see thin ice along the coast (up to 30 cm thick) and around the islands and two tongues of the Arctic ice sheet stretching south to the Laptev Sea. A small area of open water is seen within the western part of the large ice sheet, close to the coast.

There are some differences between the situation described by the two algorithms. The TTI algorithm described in this report shows the central Laptev Sea to contain thin ice, while the SMOS estimate shows that it is mainly ice free. The SMOS result also shows ice with a thickness of about 15 cm in the part of the northern ice sheet, while TIM estimated it up to 30 cm thick. In general TTI tends to estimate more and thicker ice than what is indicated by the SMOS estimate.

However, although differences exist between the two estimates, they mostly agree on general aspects. They both agree on where the ice is thick and where it is thin. With the exception of some areas in the central Laptev Sea they show the same areas to be ice covered. It is clear that there is correlation between the two estimates in general.
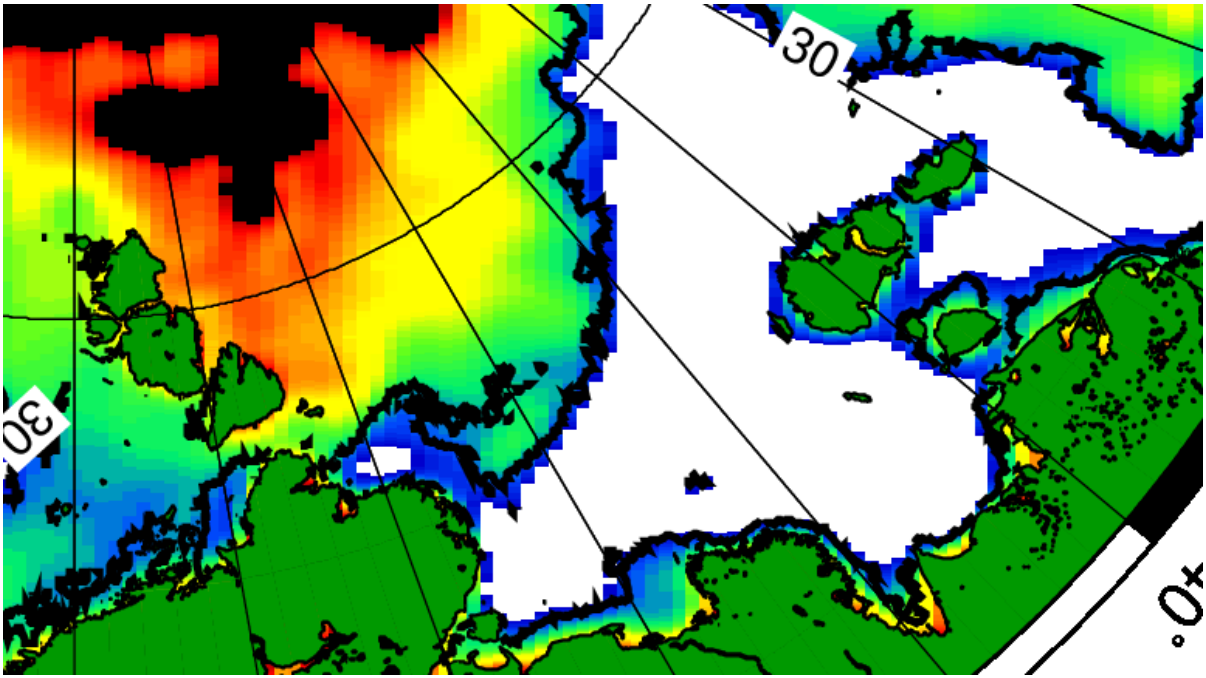
Figure 6.8: Thin ice thickness estimate with SMOS, October 13, 2010. Zoomed in on Laptev Sea (Wang & Heygster, 2011)

7 Discussion and potential improvements

The agreement between the TTI and sea ice concentration maps shows that the algorithm described in this note is capable of estimating the extent of thin sea ice. The comparison with TIM also suggests that it is capable of giving an indication of the thickness of sea ice, although the accuracy of this estimate is difficult to evaluate at this stage, without available in situ measurements.

However, the results also reveal certain challenges which need to be addressed. The most obvious one is the poor cloud masking of night images. One possible solution is to develop a cloud masking algorithm specialized for use in Arctic coast areas during night. Another approach would be to use daytime images, by accounting for the solar radiation. As described in section 5.2 the cloud masking is significantly better for the daytime images. Even for severe meteorological conditions the pollution from unmasked clouds is small. However, proper modelling of the short wave heat flux is challenging and introduces larger errors into the estimate. If daytime images are to be used, these errors need to be reduced.

Another source of errors is illustrated by the ice concentration maps. A large fraction of the area may have only fractional ice coverage within a pixel. Both the TTI and TIM algorithms described in this note assume a homogeneous ice coverage, and the presence of open water and ice within the same pixel will yield an incorrect result. A solution to this could be to use the ice thickness estimates together with sea ice concentration estimates, to indicate the reliability of the ice thickness estimate. In areas where the sea ice concentration is low, the ice thickness estimate is probably influenced by the presence of open water. It should be pointed out that the sea ice concentration maps have a resolution of 6.25 km, compared to the 1 km resolution of the MODIS data, so the problem may not be as severe as the images may suggest.

Other types of heat fluxes should be included. The assumptions of vanishing latent heat flux and sensible turbulent heat flux are maybe good enough for a first approximation, but are nonetheless a source of error, and should be some of the first aspects of the algorithm to be improved. The comparison with the thin ice thickness estimates of SMOS shows that the algorithm is sensitive to the thickness and extent of sea ice, although with a low accuracy. This can be improved by extending the model to account for other types of heat fluxes.

The TTI algorithm also has potential for a series of small improvements which could be implemented with, probably, relatively small effort. This includes improving (or replacing) some of the various empirical models used in the algorithm. It would also be beneficial to transform the results to some standard projection. This would facilitate comparison with other images and results (for example with sea ice concentration maps). Also, the artefacts appearing in figures 6.2-6-4 should be addressed.

Several of the variables usable in this model can be acquired from the ERA interim data. The program already makes use of ERA data, and more variables could relatively easily be included. In particular, this will be useful when extending the model to include other types of heat fluxes.

The algorithm for the daytime images, with a model accounting for the solar radiation heat flux, generally agrees with the algorithm for night images early in the winter when the ice is thin.

However, later, when the ice is thicker the daytime algorithm shows errors (too thick ice) and breaks down (finds no valid solution). This may be caused by inaccuracies in the estimates of albedo or transmittance. The error could also be related to the empirical model for snow thickness, since both the albedo and transmittance depend on this.

If the error originates from the estimate of albedo or transmittance, the algorithm could be improved by solving the equation for ice thickness, using the full parameterisations of albedo and transmittance. In this case an analytical solution is not feasible, but a numerical scheme could be implemented.

8 Conclusions and recommendations

Based on the agreement with other observations of ice concentration in the area, we conclude that the TTI algorithm is able to estimate the extent of thin ice the Sea of Okhotsk. The results show a cover of ice expanding throughout the winter according to expectation. By the end of the time period studied it shows that most of the sea is covered with ice, in agreement with other observations.

The TIM mask also expands through the year, although slower. It masks areas which have been covered by ice for a while. There is an agreement between the areas masked by TIM and the areas estimated to be thick by TTI, indicating that both of the algorithms detect thicker ice. However, more testing is needed to establish exactly which property of the ice triggers the TIM. It should be pointed out that the TIM provides relatively stable results, independent of cloud cover, which provides a valuable complement to the TTI.

The accuracy of the ice thickness estimates by the TTI algorithm is difficult to assess without comparing with ice thickness observations. Based on the agreement with TIM described above it is clear that TTI is sensitive to sea ice thickness. The cross check with the ice thickness estimates from SMOS indicate the same. However, the test results should, where possible, be confronted with actual in situ measurements of ice thickness in order to establish the accuracy of the estimates.

Although in situ measurements are so far not available, we see from other comparisons that the results are sensitive to the extent and thickness of thin sea ice, but with a low accuracy. Modelling of the remaining heat fluxes would improve on the accuracy and should be implemented.

The greatest challenges demonstrated by these results are the poor cloud mask for night images and the low accuracy of the daytime images. This presents us with the dilemma of whether to focus further development of the algorithm on night or daytime images.

For the night images, the choice of cloud masking algorithms is limited. The quality of the currently used cloud mask is poor in the regions relevant for this project (Arctic coast), and this severely reduces the reliability of the TTI, which relies on the thermal bands. Developing a cloud mask algorithm for Arctic coastal regions during night should be considered.

For the daytime algorithm the cloud masking is significantly improved, but at the cost of reduced accuracy in the ice thickness estimates, especially when the ice grows thick. Solving the equations for the ice thickness numerically would improve the accuracy of the estimate.

The TIM and TTI algorithms have shown to provide efficient methods for estimating the extent of thin sea ice from large data sets, and provide an indication of the ice thickness. Although confrontation with in situ ice thickness measurements is needed, they show promise already at this stage.

9 References

Amlien, J. and R. Solberg, 2003. A comparison of temperature retrieval algorithms for snow covered surfaces. IGARSS 2003, Toulouse 21.-25. July 2003.

ACIA, 2005. *Arctic Climate Impact Assessment - Scientific Report*. Cambridge University Press.

Bisht, G., Venturini, V., Islam, S., Jiang, L., Estimation of the net radiation using MODIS (Moderate Resolution Imaging Spectroradiometer) data for clear days, *Remote Sensing of Environment*, 97 (2005) 52

Comiso, J.C., D.J. Cavalieri, C.L. Parkinson and P. Gloersen, 1997. Passive microwave algorithms for sea ice concentration: A comparison of two techniques. *Remote Sensing of the Environment* 60, 357–384.

Comiso, J.C., 2002. A rapidly declining Arctic perennial ice cover. *Geophys Res. Lett.*, 29(20), 1956.

Drucker, R., S. Martin and R. Moritz, 2003. Observations of ice thickness and frazil ice in the St. Lawrence Island polynya from satellite imagery, upward looking sonar, and salinity/temperature moorings. *Journal of Geophysical Research*, 108 (C5), 3149.

Grenfell, T. C., 1979. The Effects of Ice Thickness on the Exchange of Solar Radiation over the Polar Oceans. *Journal of Glaciology*, 22, 305

Key, J., J. Collins, C. Fowler, and R. Stone, 1997. High-latitude surface temperature estimates from thermal satellite data. *Remote Sensing Environ.*, 61, 302-309.

Maykut, G. A., 1978. Energy Exchange Over Young Sea Ice in the Central Arctic. *Journal of Geophysical Research*, 83 (C7), 3646.

Maykut, G. A., 1982. Large-Scale Heat Exchange and Ice Production in the Central Arctic. *Journal of Geophysical Research*, 87 (C10), 7971.

Oliver, J.E., 2005. *The Encyclopedia of World Climatology (Encyclopedia of Earth Sciences)*. Springer Verlag.

Spreen, G., L. Kaleschke, and G. Heygster, 2008, Sea ice remote sensing using AMSR-E 89 GHz channels, *Journal of Geophysical Research*, doi:10.1029/2005JC003384

Svendsen, E., Maetzler, C., Grenfell, T., 1987. *International Journal of Remote Sensing*. Vol. 8, pp. 1479-1487

Tucker, W.B., J.W. Weatherly, D.T. Eppler, D. Farmer, and D. Bentley, 2001. Evidence for the rapid thinning of sea ice in the western Arctic Ocean at the end of the 1980s. *Geophys. Res. Lett.*, 28(14), 2851-2854.

Wang, H., Heygster, G. , 2011, Private communication

Wessel, P., and W. H. F. Smith, A Global Self-consistent, Hierarchical, High-resolution Shoreline Database, 1996, *J. Geophys. Res., 101, #B4, pp. 8741-8743*

Yu, Y. and Rothrock, D. A., 1996. Thin ice thickness from satellite imagery. *Journal of Geophysical Research,* 101 (C10), 25753.

Zillman, J. W., A study of some aspects of the radiation and heat budgets of the southern hemisphere oceans, *Meteorol. Stud.*, 26, Dep. Interior, Canberra, 1972.